The Pnictogen Bond Forming Ability of Bonded Bismuth Atoms in Molecular Entities in the Crystalline Phase: A Perspective

Pradeep R. Varadwaj [1,2,*], Arpita Varadwaj [1],* Helder M. Marques [2] and Koichi Yamashita[1]

[1]Department of Chemical System Engineering, School of Engineering, The University of Tokyo 7-3-1, Tokyo 113-8656, Japan
[2]Molecular Sciences Institute, School of Chemistry, University of the Witwatersrand, Johannesburg 2050, South Africa

SUPPLEMENTARY INFORMATION[1]

S.A. Inter- and intra-molecular interactions and the sum of the van der Waals radii criterion

Historically,[1] and also more recently,[2-5] the *less than the sum of the van der Waals radii* concept has been widely utilized to identify and characterize non-covalent interactions in molecules, molecular complexes, and crystals.[6-10] Based on this concept, when the inter- or intra-molecular interaction distance in a molecular or supramolecular entity is less than the sum of the van der Waals (vdW) radii of interacting atomic basins, they should be regarded as being non-covalently bonded to each other. This is seen as a necessary – but not necessarily sufficient – condition for a non-covalent interaction.

Some have found the criterion is actually an impediment in the search for non-covalent interactions;[11] others have argued that it is very useful for rationalizing such interactions in chemical systems, including molecules, molecular complexes, and crystals. So, Alvarez observed that the vdW radii and associated vdW surfaces are extensively used for crystal packing and supramolecular interaction analysis.[4] Politzer and Murray,[12] and others,[4, 13] have argued that where the Pn···D inter- or intramolecular distance exceeds the sum of the vdW radii by several tenths of an Ångstrom in a crystal system, this can still be recognized as a non-bonded interaction. This is understandable since values proposed for the vdW radii of atoms have a typical uncertainty of ± 0.2 Å;

[1] References refer to material in this Supplementary Information and are given at the end of this document.

hence "less than the sum of the vdW radii" concept will necessarily miss a significant number of non-covalent interactions if treated as a strict criterion to identify a non-covalent interaction. This uncertainty is not surprising since a hard sphere model with spherical symmetry of electron density was assumed in proposing the vdW radii of atoms. In reality, the charge density profile of atoms in molecules is anisotropic, and hence the vdW "radius" of an atom in a molecular entity is likely to vary between molecular entities. Chernyshov and co-workers[14] have recently attempted to describe an efficient and universal approach for the analysis of non-covalent interactions and determination of vdW radii using the line-of-sight (LoS) concept. The authors argued that this approach is able to unambiguously identify and classify the "direct" interatomic contacts in complex molecular systems, and hence is an improved theoretical base to molecular "sizes" but also enables the quantitative analysis of specificity, anisotropy, and steric effects of intermolecular interactions.

S.B. Directionality

As mentioned before,[9, 10] and reproduced here for the reader's convenience, to maximize the integrity of our identification and subsequent characterization of pnictogen bonding in the crystal systems examined, we took into account the angle of interaction.

The putative site of interaction on donor D was inspected to determine whether it was indeed a nucleophilic or an electrophilic domain. Type-I interactions (Scheme 1a), which can be subdivided into Type-Ia and Type-Ib, appear when the regions of the interacting atomic domains have either both a positive or negative local polarity. They are non-linear interactions, and non-directional. There are many chemical systems deposited in the CSD where the angles θ_1 and θ_2 (Scheme 1a, left) are virtually equal (and range between 110° and 150°), and should therefore be regarded as Type-Ia (trans) depending on the charge polarity of both Pn and D in the R–Pn···D motif. For a Type-Ib topology of bonding to appear between interacting atomic domains in chemical system, the angles θ_1 and θ_2 should be reasonably different from one another, thus following a configuration similar to that depicted in Scheme 1a (right).

The angle θ of approach, θ = ∠R–Pn(Bi)···D, of the electrophilic region on the electrostatic surface of Bi towards the nucleophilic region of the donor, D, was determined and classified as a linear, quasilinear, or bent (non-linear) interaction. There could be three σ-holes, for instance, along the extensions of three covalently/coordinately bound R–Bi bonds in a molecular entity containing a trivalent bismuth, so there would be three angles between the electrophiles on bismuth and D.

The angle, θ, corresponding to each of the three R–Bi···D σ-hole interactions may follow a common Type-IIa pattern of bonding (Scheme 1b, left).

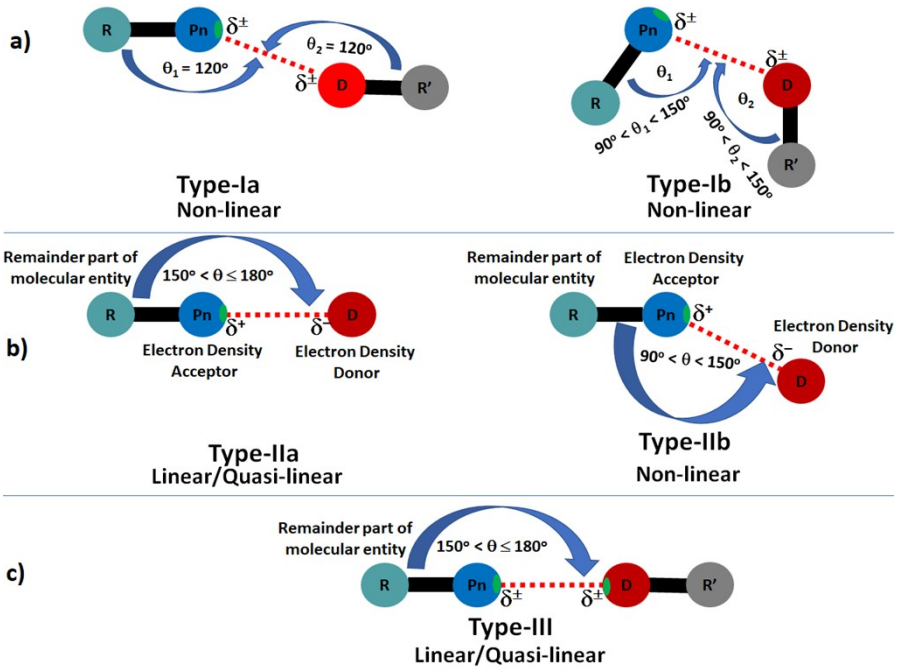

Scheme S1. A schematic view of a) Type-I, b) Type-II and c) Type-III topologies of non-covalent bonding interactions (Pn = Bi in this case). The θs represent the angle of interaction between the interacting atomic domains, and Pn (i.e., Bi in this case), D, R and R' refer to the covalently bound pnictogen atom, the interacting atomic domain (generally nucleophilic), and the remaining part of the molecular entities associated with Pn and D atomic basins, respectively. $\delta^{\pm}$ signifies the local polarity (positive or negative), and the small region on atom Pn along R–Pn bond extension colored in green indicates a σ-hole. This classification scheme has been discussed elsewhere.[15, 16]

The directional interactions that are linear or quasi-linear generally follow a Type-IIa topology of bonding (Scheme 1b, left). This is a topology of bonding that typifies the name "pnictogen bonding"; the topology also resembles hydrogen bonding, halogen bonding, chalcogen bonding and so on, in which a positive site on a covalently bound atom (in this case hydrogen, halogen, and chalcogen and so on) is linearly/quasi-linearly in attractive engagement with a negative site on another site on the same or on a different molecular entity. As such, the interaction is linear when $\theta = \angle$R–Pn···D = 180°, and quasi-linear when 150° < θ < 180°. In either case, the electrostatic surface of covalently bound Bi must feature an electrophilic region along the extension of the R–Bi covalent or coordinate bond, and D is a Lewis base (such as N in NH_3, O in OH_2, and F in HF). There could be exceptions, for example, when the angle θ < 150°, but the covalently bound Pn atom (Bi this case) in a molecular entity that has an electrophile on

it is non-linearly attracting a negative site on an interacting molecular entity. Thus, when $90^{o} < \theta < 150^{o}$, and the electrostatic surface of Bi still features a positive region, we recognize the interaction as being of Type-IIb. Both Type-IIa and Type-IIb interactions are of coulombic origin.

Type-III interactions occur when the angle of interaction follows a Type-IIa topology of bonding, but the interacting regions on Pn and D are either both positive or both negative. This type of interaction occurs not only between anions, or between cations, in chemical adducts in the crystalline phase, but also in chemical systems, in which two covalently bound positive Bi atoms in molecular entities attract each other due to differences in the charge density on their electrostatic surfaces (see succeeding sections for examples).

S.C. Computational approaches

The following section contains several illustrative crystal systems retrieved from CSD or ICSD to highlight instances where bismuth bonding can be anticipated. In order to provide insight into evidence of Bi-centered pnictogen bonding formed by Bi containing molecular entities and the negative site in interacting species, a few systems were considered for the calculation of Molecular Electrostatic Surface Potential (MESP). The simplest chemical systems chosen include the bismuth trihalides, BiX_3 (X = F, Cl, Br, I), trimethyl bismuth, $Bi(CH_3)_3$, and molecular Bi, Bi_2.

Electronic structure calculations at the MP2 level theory,[17, 18] in conjunction with def2-TZVPPD pseudopotential basis set,[19] were performed to obtain their equilibrium geometries. Normal mode vibration analysis was performed for each of the six systems mentioned above and positive eigenvalues were found. We then calculated the resulting wavefunctions at the same level of theory to compute the electrostatic surface potential of the molecular entities. The Gaussian 16 suite of programs was used.[20] The 0.001 *a.u.* (*electrons* $Bohr^{-3}$) *isoelectron density* envelope that arbitrarily defines the vdW surface of a molecular entity was used on which to calculate the potential. As has been shown many times,[7-10, 21-24] the application of the MESP model to a molecular entity results in two types of extrema called the local most minimum and the local most maximum of potential ($V_{S,min}$ and $V_{S,min}$, respectively) that appear on the molecular surface. The sign of both $V_{S,min}$ and $V_{S,min}$ could either be positive, or negative, or sometimes even neutral. When it positive, it is generally assumed that the region on the surface that accompanies this is electrophilic, and hence may be suitable for accepting electron density from an interacting electron donor in close proximity. When it is the negative, that the region is nucleophilic, and hence may be capable of donating electron density to an interacting electrophile in its vicinity. However, it should be kept in mind

that all negative or positive sites on the surface of the molecular entity may or may not always be capable of engaging in attractive interaction with a region that features the opposite reactivity profile. The usefulness of the MESP model to understand the surface reactivity has been demonstrated on many occasions (for example[25-28]).

The theoretical details of the promolecular charge density-based IGM model called IGM-δ*g* has been discussed elsewhere[29, 30] and its usefulness in understanding intra- and inter-molecular interactions in chemical systems has been demonstrated many times (for example[7-10, 15]). Since this model can separate intramolecular and inter-fragment interactions in a molecular entity, one can plot this in two (spikes) or three dimensions (isosurface volumes) to reveal the presence and nature of intramolecular or intramolecular interactions between bonded atomic basins in molecular entities. From the shape of the isosurface volume, we can infer the localized or delocalized nature of the interactions involved between interacting domains, and the charge density responsible for the shape of the volume is a measure of strength of the interaction. The colors of these volumes, blue and green, generally represent strong and weak attractions, respectively, and red represents a repulsive interaction.

As a special case, in order to clarify whether the Bi–I and B···O close contacts in host-guest complexes such as that in [BiI_3][15-crown-5], and [BiI_3][Benzo-15-crown-5], are coordinate or pnictogen bonds, we energy minimized the geometry of the two complexes in the gas phase at the [*ω*B97XD/def2-TZVPPD] level of theory. Quantum Theory of Atoms in Molecules (QTAIM)[31] calculations were performed to explore the nature of the bond path and bond critical point topologies of the charge density. Examination of this, together with that of the other three descriptors of theory, the Laplacian of the charge density, the potential energy density, and the total energy density, has enabled us to suggest that Bi–I are typical coordinate bonds and the Bi···O close contacts are pnictogen bonds.

Analysis and drawing of geometries of various molecular entities and crystals were performed using the Mercury 4.0[32] and VMD[33] suite of programs. AIMAll[34] and MultiWfn[35] codes were used for calculation and analysis of MESP and QTAIM graphs, and VMD [33] was used for drawing of IGM-δ*g* based isosurfaces.

S.D. Bismuth in Crystallography: Materials Design and Discovery

Bismuth compounds have played a very significant role in the development of many functional materials,[36, 37] including photocatalysts and photovoltaics. Our constrained search (*R*-factor ≤ 0.1) of the R–Bi geometrical motif in the CSD resulted in 4924 (5026) hits that feature Bi in its variable oxidation states; the parenthesis value was obtained from an unconstrained CSD search; R represents any atom of the periodic table. Fig. S1 illustrates the frequency of appearance of such crystals in terms of the number of publications per year. It shows a systematic increase in the number of publications with respect to time, with very significant growth in the last five years.

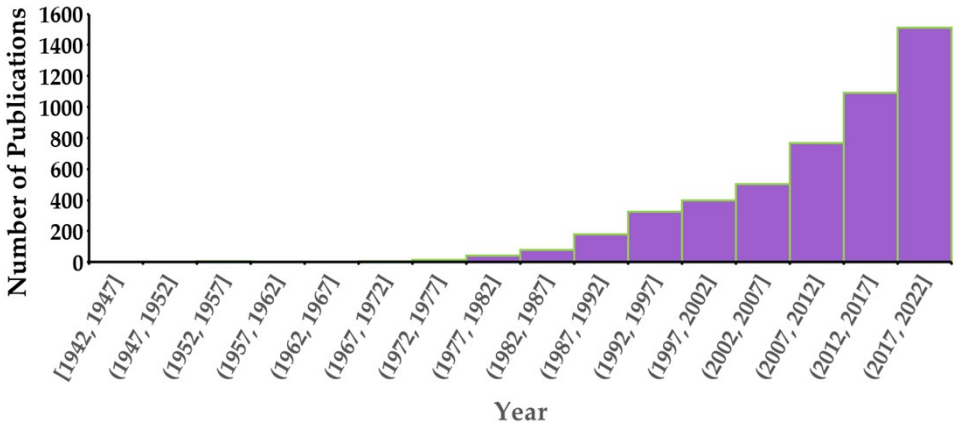

Figure S1. A histogram showing a systematic growth in the number of publications of crystalline solids containing the element Bi. CSD (version 5.43 updates (July 2022)) search gave 4924 single crystals that contain Bi.

Although the solid state structure of many bismuth compounds have been reported, the basic chemical reactivity of Bi when forming complexes in the solid state is yet to be fully understood.[38] In many of these compounds, there is clear evidence of the ability of Bi to engage in non-covalent interactions when in suitable proximity to a nucleophilic site.

Illustrated in Fig. S2 are a set of crystals containing covalently or coordinately bonded Bi; in some Bi is involved in forming bismuth bonds, but not in others, thus featuring the variability in the nature of coordination/interaction modes of Bi in molecular entities. In the first two geometries shown in Figs. 2a and 2b, Bi in one electrically neutral molecular entity (viz. as in $C_{22}H_{21}BiBrN$) interacts favorably with an equivalent Bi in an identical neighboring entity to form a Bi-centered pnictogen bond,[39] including the involvement of a Bi···π(arene) interaction. In these systems, bismuth bonds occur between the coordinately bonded Bi atoms; they are long-ranged, and quasi-

linear. The quasi-linear nature of the Bi···Bi interaction may arise from repulsion between the Bi atoms causing a mutual shift to positions where they can maximize their mutual attraction. This suggests that the positive region on the electrostatic surface of Bi in one molecular entity is in an attractive engagement with the positive region on Bi in another similar molecule that has a different charge density. The Bi···Bi interaction is therefore a Type-III interaction (Scheme 1c of the text).

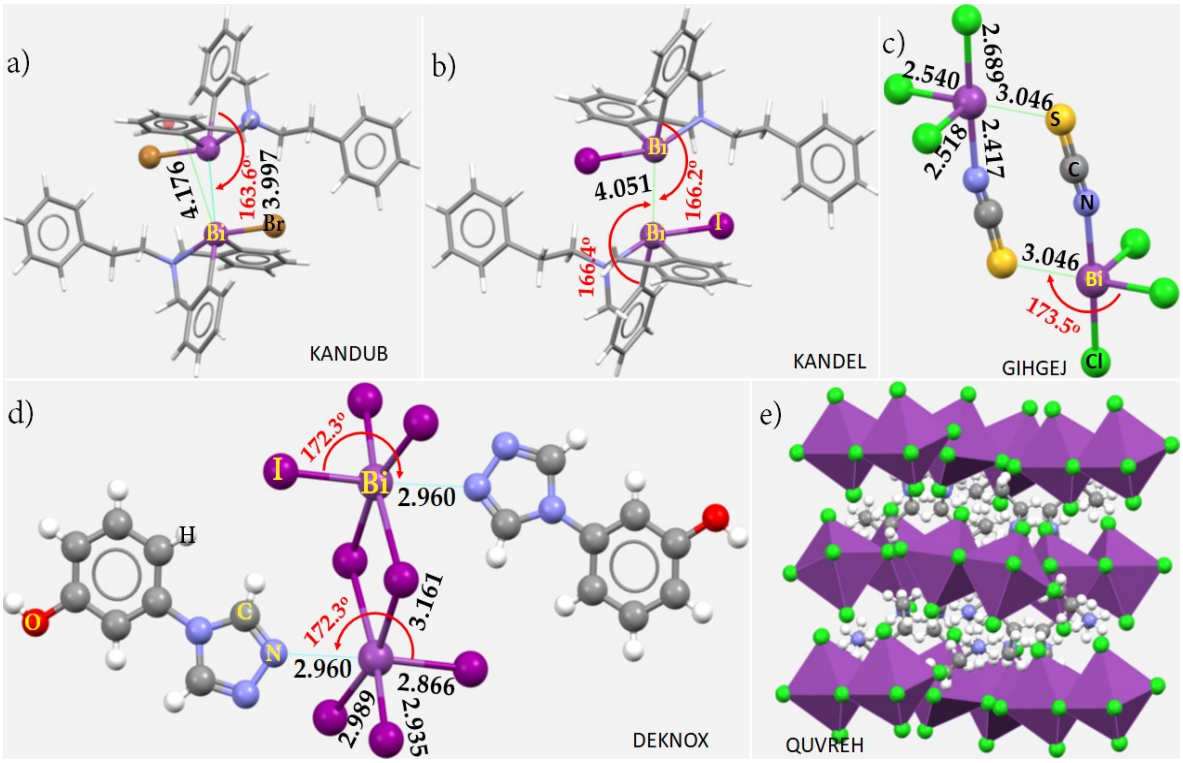

Figure S2. Illustration of Bi-centered non-covalent interactions in some chemical systems. a) (2,2'-[[(2-phenylethyl)azanediyl]bis(methylene)]di(benzen-1-yl))-bromo-bismuth(III) ($C_{22}H_{21}BiBrN$);[39] b) (2,2'-[[(2-phenylethyl)azanediyl]bis(methylene)]di(benzen-1-yl))-iodo-bismuth(III) ($C_{22}H_{21}BiIN$);[39] c) (18-crown-6)-potassium trichloro-isothiocyanato-bismuth(II) ($C_{12}H_{24}KO_6^+$,$CBiCl_3NS^-$);[40] d) bis((*m*-phenol)-1,2,4-triazolium) bis(*m*-phenol)-1,2,4-triazole bis(μ_2-iodo)-hexaiodo-di-bismuth ($2(C_8H_8N_3O^+)$,$Bi_2I_8^{2-}$,$2(C_8H_7N_3O)$);[41] e) bis(propylammonium) bis(μchloro)-octachloro-bismuth(III) ($4(C_3H_{10}N^+)$,$Bi_2Cl_{10}^{4-}$).[42] Selected bond distances and bond angles are in Å and degrees, respectively. The CSD reference is shown for each case in upper-case letters. 18-crown-6-potassium in c) was removed for clarity. Selected atom types are marked.

In Fig. S2c, which illustrates part of the crystal of $[C_{12}H_{24}KO_6]^+[CBiCl_3NS]^-$,[40] the Bi···S close contact is not a Type-IIa pnictogen bond since the charges on Bi and S are both negative, even though the directional feature is satisfied. The intermolecular distance associated with this interaction (r(Bi···S) = 3.046 Å) is significantly longer than the formal Bi–N and Bi–Cl coordinate bonds (r(Bi–Cl) = 2.540 Å; r(Bi–Cl) = 2.689 Å; r(Bi–

Cl) = 2.518 Å; *r*(Bi–N) = 2.417 Å) that occur in the $[CBiCl_3NS]^-$ anion. Because the Bi···S close contact appears along the Cl–Bi bond extension, and is substantially longer than the other four coordinate bonds, we recognize this $Bi^{\delta-}\cdots S^{\delta-}$ close contact to be a Type-III pnictogen bond. By the same logic, the $Bi^{\delta-}\cdots S^{\delta-}$ close contact in Fig. S2c is also a Type-III interaction. In case of the organic-inorganic hybrid structure, $(2(C_8H_8N_3O^+),Bi_2I_8^{2-},2(C_8H_7N_3O))$, shown in Fig. S2d,[41] Bi is hexacoordinate and one of the Bi(III) ions is involved in a Bi···N close contact; while ∠I–Bi···N is quasi-linear, it may be a nitrogen-centered Type-IIb N···Bi pnictogen bond since ∠C–N···Bi is non-linear (∠C–N···Bi = 127.6°), and since Bi in $Bi_2I_8^{2-}$ acts as an electron density donor while N in the interacting organic cation is positive. Although the Bi–I bond distances in Fig. S2d are comparable to the Bi···N bond distance, the latter is clearly a nitrogen-centered pnictogen bond, whereas the former is a coordinate bond. This is understandable given that the vdW radius of I is substantially larger than that of N (r_{vdW} (N) = 1.66 Å; r_{vdW} (I) = 2.04 Å).

The bonding topology shown in Figs. 2a-d is not the same as in found in the crystal of $4(C_3H_{10}N^+)\cdot Bi_2Cl_{10}^{4-}$, Fig. S2e,[42] where each Bi is coordinated by six chloride ions, forming a corner-shared octahedron, leading to the formation of a 2D inorganic layered framework; the organic cation connects the inorganic layers via a network of H···I hydrogen bonds and other non-covalent interactions, giving stability to the overall geometry of the 2D system. Given the coordination geometry of Bi(III), we found no evidence for a bismuth bond in this crystal. It is worth noting that the polynuclear $[Bi_2I_8]^{2-}$ anion in the organic-inorganic hybrid system in Fig. S2d consists of two BiI_5 square pyramids as inorganic layers. The compound is a semiconducting material since the experimentally determined optical absorption spectra features a sharp optical bandgap of 2.07 eV. Comparable properties were observed for similar compounds, viz. $[HL_1]_4[Bi_6I_{22}]\cdot[L_1]_4\cdot 4H_2O$ (L_1=3-(1,2,4-triazole-4-yl)-1H-1,2,4-triazole); $[HL_2]_4[Bi_6I_{22}]\cdot 6H_2O$ (L_2=(*m*-phenol)-1,2,4-triazole). These comprise polynuclear $[Bi_6I_{22}]^{4-}$ anions to build up the inorganic layers and substituted 1,2,4-triazoles as the organic layers. There exist several hydrogen bonding and I···I halogen-halogen bonded interactions in all these three structures, and that they feature optical gaps of 1.77, 1.77, and 2.07 eV, respectively. These demonstrate that a basic understanding of pnictogen bonds in chemical systems is necessarily required since their presence enables compounds to behave as semiconductors; they therefore should be taken into account in the *de novo* design of functional materials.

A search of the ICSD and CSD databases produced thousands of compounds containing Bi, in which, Bi^{3+} has a flexible coordination number that is usually anywhere between 3 and 10.[43] Coordination to π systems is not unusual. For instance, the

compound [$BiCl_3$(1,2,3-$Me_3C_6H_3$)] contains quasi-dimeric units of arene-coordinated $BiCl_3$ fragments that are further associated *via* additional Bi–Cl contacts to form coordination-polymeric layers. In this system, Bi^{3+} has three primary coordinate bonds with Cl^-, three secondary contacts, and is associated with an arene moiety. The Bi-arene bonding in this crystal is characterized by Bi–C distances in the range 3.168 (7)-3.751 (8) Å [44], suggesting η^6 coordination of the Bi^{3+} ion with the arene. Another example is its π bonding to a pyrrole ring in the compound 5,10,15,20-tetraphenylporphyrindium dibromo-trichloro-bismuth (CSD refs. EPAQOE and EPARUL, Fig. S3a[45]). An example of 4, 6 and 10 coordinated Bi^{3+} is in the crystal of the 2-amino-4-methylpyridinium tetrachloro-bismuth (Fig. S3b), octakis(pyrrolidin-1-ium) hexachloro-bismuth (μ-chloro)-decachloro-di-bismuth dihydrate (CSD ref. AKEMUB; Fig. S3c) and polyoxopalladate, Na_7[Bi(III)$Pd_{15}O_{40}(PPh)_{10}$]·$39H_2O$ (CSD ref. NADDAB)[46]), respectively.

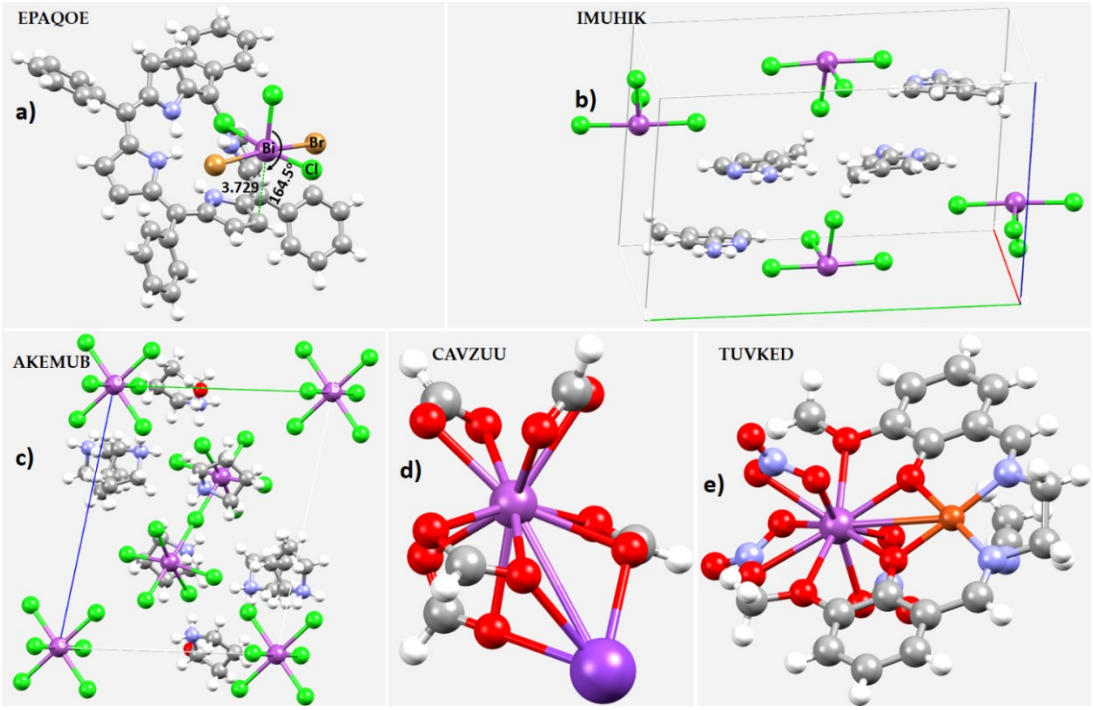

Figure S3. Examples illustrating the diverse coordination modes of Bi in crystals: a) 5,10,15,20-tetraphenylporphyrindium dibromo-trichloro-bismuth (CSD refs: EPAQOE and EPARUL [45]); b) 2-amino-4-methylpyridinium tetrachloro-bismuth (CSD ref: IMUHIK [47]); c) octakis(pyrrolidin-1-ium) hexachloro-bismuth (μ-chloro)-decachloro-di-bismuth dihydrate (CSD ref. AKEMUB [36]); d) dipotassium (pentaformato-O,O')-bismuth (CSD ref: CAVZUU [48]); e) (μ-2,2'-[ethane-1,2-diylbis(azanylylidenemethanylylidene)]bis(6-methoxyphenolato))-tris(nitrato)-copper(II)-bismuth(III) acetonitrile solvate (CSD ref. TUVKED [49]). The Bi…π(C=C) bond length and ∠Cl–Bi…C bond angles are indicated only for the structure shown in a) to clarify that there is probably tetrel bonding between Bi and π(C-C)-moieties, and there is no pnictogen bond in this system since Bi is entirely negative in $[BiBr_2Cl_3]^{2-}$.

Higher coordination numbers of Bi are certainly known; crystals such as the potassium salt of the pentaformate complex of Bi^{3+} (Fig. S3d)[48] and a bimetallic Cu^{2+}, Bi^{3+} salen complex, possibly featuring bonding between the two metal ions (Fig. S3e),[49] are examples. Three types of Bi–M bonding are known in transition metal complexes displaying a bismuth species in the coordination sphere of the transition metal M: dative Bi→M interactions (with Bi acting as a donor), dative Bi←M interactions (with Bi acting as an acceptor), and covalent Bi–M interactions.[50] The nature of Bi–M bonding, trends in the geometric parameters, and in the coordination chemistry of the Bi-containing compounds have been reviewed, focusing on the reactivity of bismuth species in the coordination sphere of transition metal complexes in stoichiometric and catalytic reactions.[50]

Our study does not consider the transition metal coordination chemistry of Bi, per se. We have just highlighted the coordination ability of Bi in some chemical systems in Fig. S3 to demonstrate below that a coordinately bound Bi site in molecular entities has an exceptional potential to engage with a versatile number of electron density donors to form pnictogen bonds.

S.E. Statistical analysis of bismuth bonds in crystal lattices

We considered the electronegative elements D = O, N, F, Cl, Br, I, S, Se, and Te, as well as $C_6(\pi)$ in arene moieties, as potential electron density donor sites in molecular entities for covalently bonded Bi to gauge the extent of occurrence of Bi···D close contacts in the crystals deposited in the CSD. Our searches involved intermolecular interactions in crystals, comprising the geometric motifs such as R–Bi···D. The geometric data (the bond distance, r(Bi···D), and the bond angle, ∠R–Bi···D) obtained from the CSD searches were statistically analyzed to determine the range of intermolecular distances and directional features for a variety of donor sites for a bismuth bond. Our search was limited to intermolecular distances between 2.6 and 4.5 Å in most cases, and bond angles between 140° and 180°. Only single crystals were selected that were free of errors and distortions, and that had an *R*-factor ≤ 0.1. The geometric fragments R–Bi···D–R′ and R–Bi···D were chosen for the searches (R′ = any element; D = selected elements of Groups 15, 16, and 17 and included carbon in aromatic rings; the bond between D and R′ was of any type). The upper limit of the intermolecular distance was chosen depending on the sum of the vdW radii of Bi and D, with a flexibility of ±0.2 Å.

The charge on Bi in the crystals resulted from our searches was either (formally) positive, neutral, or negative. For instance, the Bi···O interactions in the crystal, $(C_8H_{20}N^+)_2$ $(C_{13}Bi_4Fe_4O_{13})^{2-}$,[51] was found to exist between negative potentials on the surfaces of Bi and O atoms since both are responsible for the $(C_{13}Bi_4Fe_4O_{13})^{2-}$ anion. This

is probably unavoidable during the search of this motif in crystals in CSD. If one imposes charge as a search criterion, a large number of real interactions will be missed.

Many crystals in the search for R–Bi···O resulted in close contacts that were formed between Bi and O in the building blocks that were entirely negative, and were driven by a counter ion of the crystal concerned. One such crystal, for example, is tetramethylammonium (μ_2-carbonyl)-decacarbonyl-di-bismuth-tetra-cobalt ($C_4H_{12}N^+$,$C_{11}Bi_2Co_4O_{11}^-$) (CSD ref. FOGGEN[52]), in which Bi···O distances vary between 3.5 and 3.8 Å, and ∠Co/Bi–Bi···D are in the range 145-172°. Similarly, in the tetrakis(tetraphenyl-bismuth) bis(μ_3-iodo)-tetrakis(μ_2-iodo)-decaiodo-tetra-bismuth acetone solvate crystal, [4($C_{24}H_{20}Bi^+$)($Bi_4I_{16}^{4-}$)·2(C_3H_6O)] (CSD ref: HUJCIZ[53]), the Bi···O intermolecular interaction is formed between negative Bi in $Bi_4I_{16}^{4-}$, and negative O in acetone (C_3H_6O) (r(Bi···O) = 3.094 Å and ∠C–Bi···O = 177.1°), this is probably an example of a Type-III bonding feature. Nevertheless, our statistical analysis was largely limited to the category of Type-II topology of bismuth bonds in crystals, and we manually eliminated crystals with close contacts where Bi would be intrinsically negative (as in an anion).

A. Bi···O close contacts, with oxygen as electron density donor

Our CSD search for the R–Bi···O geometric motif with r(Bi···O) in the range 2.6 – 3.8 Å and A (∠R–Bi···O) in the range 140 – 180.0° resulted in 376 single crystals with 871 close-contacts. A close inspection of these crystals revealed that Bi in 39 crystals contain 81 close contacts that occurred between negative sites and are directional. We removed them from the list since they cannot be Type-II bismuth bonds. The normal distribution of the remaining close contacts in 337 crystals is shown in Fig. S4. The results suggest that the great majority of Bi···O close contacts follow a Type-IIb topology of bonding rather than Type-IIa (Fig. S4a). The non-linearity in the Bi···O close contacts is because the fragment R' covalently attached with the donor atom O is prone to form other interactions (such as hydrogen bonds) with its nearest neighbor; the donor atom therefore shifts to a position to maximize its non-covalent interaction with Bi, resulting in a non-linear close contact. The peaks of the normal distributions occur around 155° and 3.2 Å in bond angle and bond distance, respectively. When a non-constrained search was performed with r(Bi···O) in the range 2.6 – 4.1 Å that has an upper limit of the intermolecular distance slightly longer than the sum of the vdW radii of Bi and O, 4.04 Å, and θ in the range 140 – 180.0°, the number of hits increased to 463, with 1184 close contacts; these are not shown in Fig. S4. The peaks of the normal distribution occurred at 153.5° and 3.4 Å for bond angle and bond distance, respectively. The largest

population of these features occurred in the range 142 – 153° and 2.9 – 3.3 Å, respectively; this is very similar to the constrained results shown in Fig. S4.

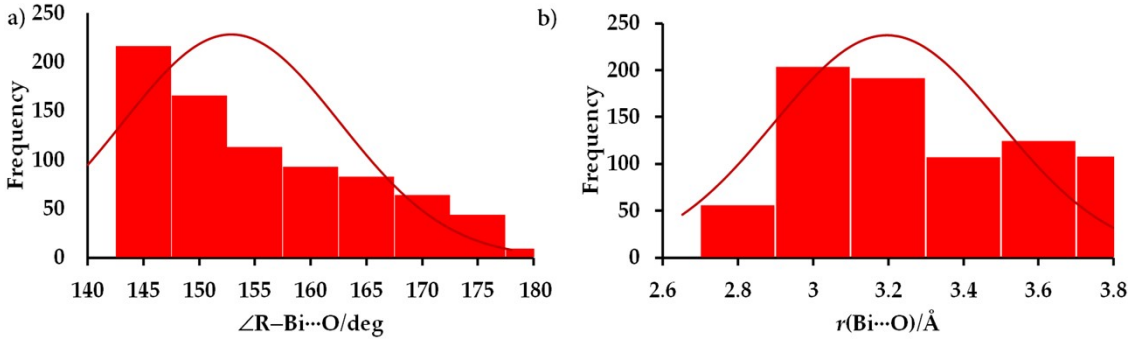

Figure S4. Histograms showing a) the angular distribution and b) intermolecular distance of 788 Bi···O close contacts in 337 crystals that emerged from a CSD search. The Bi···O intermolecular distance *r* (and intermolecular angle ∠R–Bi···O) in the range of 2.6–3.8 Å (140–180°) was used as a geometric criterion during the CSD search, where R represents any atom. Bond lengths and angles are in Å and degrees, respectively. The normal distribution curve is shown in dark-red in each plot.

B. Bi···S (Bi···Se, and Bi···Te) close contacts, with heavy chalcogen derivatives as donors

Our search of the CSD for the R–Bi···S geometric motif with *r*(Bi···S) in the range 2.6 – 4.3 Å and ∠R–Bi···S in the range 140 – 180.0° resulted in 119 single crystals with 188 close-contacts. When Se and Te were included as donors, the search resulted in 128 crystals that contain 204 close contacts, showing that the frequency of Se and Te as electron donors is quite low in forming bismuth bonds. Some of the Bi···Se and Bi···Te close contacts found in seven of these 128 crystals were not bismuth bonds since they appear between entirely negative Bi and Se (or Te) sites. For instance, the Bi···Se/Bi···Ch close contact in [$C_8H_{20}N^+$,$C_9BiFe_3O_9Se^-$] (CSD ref: COFGAI[54])/[$C_8H_{20}N^+$,$C_6BiFe_2O_6Ch^-$] (Ch = Se, Te) (CSD ref. COFGEM and COFGIQ[54]) occurs between two identical anions ($C_9BiFe_3O_9Se^-$ or $C_6BiFe_2O_6Se^-$) and is driven by the tetraethylammonium ($C_8H_{20}N^+$) cation. This is indeed different from the Type-IIa bonding topology involving a positive site on Bi and negative S as in the crystal of diphenyl-phenylselenyl-bismuthine, $Ph_2NiSePh$ (CSD ref: GIPREC[55]); *r*(Bi···Se) = 3.897 Å and ∠Se–Bi···Se = 176.8°).

In some crystal structures several close contacts occur between Bi in one unit and S in a thiacetate. We regard them as false contacts; these are actually Bi···O close contacts (as in dioxodibenzothiabismuth-phenyl acetate (CSD ref: IGESAR[56]); [(2,6-(CH_2NH_2)Me)Ph)Bi(Me)$^+$][$CF_3SO_3^-$] (CSD ref: WUXHUV[57]); [SO_2Ph_2Bi(OPh-*p*-OMe)][*p*-OMe-phenol) (CSD ref. XADQUO[58]); and [2-(*N*-phenylcarbonylamino)phenyl-Bi(py)$^{2+}$][$CFSO_3^-$] (CSD ref: YODWAS[59])). Based on these observations, 32 of the 128 crystals were rejected as having false contacts. The geometric motifs associated with the

Bi···Ch (Ch = S, Se, Te) close contacts in the remaining 96 crystals are plotted in Fig. S5, based on 156 close contacts. As can be seen, no close contacts were found below 3.0 Å. The normal distribution shows that the largest occurrence of *r*(Bi···S) and ∠R–Bi···S and is in range 3.4 – 4.0 Å and 150 – 170° and, respectively, with the peak of the normal distributions of corresponding geometries at 3.6 Å and 157°, respectively.

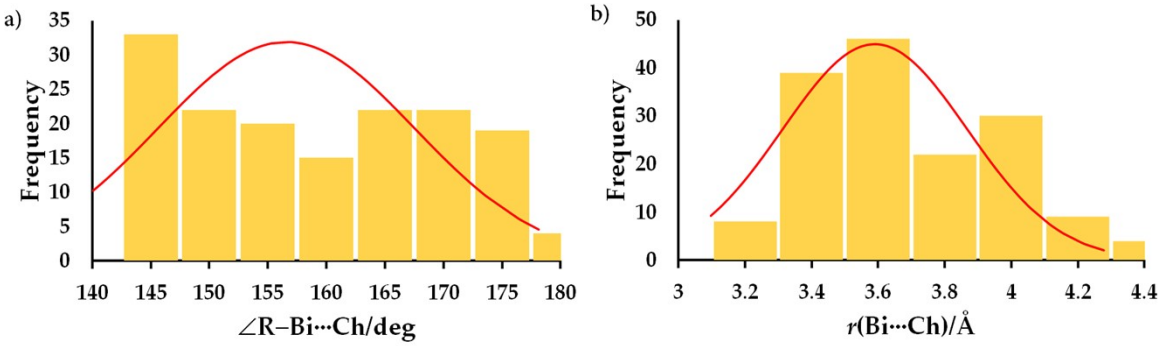

Figure S5. a) and b) Histograms showing, respectively, the angular and intermolecular distance distributions of 157 Bi···Ch (Ch = S, Se, Te) close contacts in 96 crystals that emerged from a CSD search. The Bi···Ch intermolecular distance *r* (and intermolecular angle ∠R–Bi···Ch) in the range of 2.6–4.3 Å (140–180°) was used as a geometric criterion during the CSD search, where R represents any atom. Bond lengths and angles are shown in Å and degrees, respectively. The normal distribution Bell curve is shown in dark-red in each plot.

C. Bi···N close contacts, with pnictogen nitrogen as donor

A search for Bi···N close contacts in the CSD gave 64 crystals. The occurrence of close contacts was examined based on the search criteria set at *r*(Bi···N) = 2.6 – 3.8 Å and ∠R–Bi···N = 140 – 180.0°. To give an example, our search gave a Bi···N close contact between the negative Bi site in pentacyano-bismuth and the negative N in CH_3CN in the crystal of $(N(PPh_3)_2^+)_2(Bi(CN)_5^{2-})\cdot CH_3CN$ (CSD ref: UBIQUU[60]), in which *r*(Bi···N) = 3.136 Å and ∠C–Bi···N = 157.5°. Similarly, we found Bi···N close contacts between Bi in $Bi_2I_8^{2-}$ and N in the μ-phenol-1,2,4-triazolium cation ($C_8H_8N_3O^+$), in the crystal structure of $[C_8H_8N_3O^+)_2][Bi_2I_8^{2-}]\cdot 2(C_8H_7N_3O)$ (CSD ref. DEKNOX[41]), in which, *r*(Bi···N) = 2.960 Å and ∠I–Bi···N = 172.3°); this is a charge-assisted N-centered pnictogen bond. We rejected this and other such close contacts from the list of close contacts in 64 single crystals. In addition, we also rejected several Bi···N false contacts found between N in nitrate and Bi in the partner cation that showed up because of the angular flexibility; in fact it is O of the nitrate anions that is linked non-covalently with Bi, as in, for example, $[Bi(Ph)_4(OH_2)^+][Bi(Ph)_4^+][Bi(Ph)_4(ONO_2)][NO_3^-]_2$ (CSD ref: VUZFEE[61]). Consequently, 24 crystals with 45 false contacts were not included in the histograms shown in Fig. S6. The population of ∠R–Bi···N is predominantly the range 150 – 175°, and there are only

a few crystals that feature ∠R–Bi···N between 175 and 180° (Fig. S6a). Similarly, the histogram plot in Fig. S6b indicates that Bi···N close contacts span the range between 2.8 and 3.8 Å, with most contacts between 3.1 and 3.7 Å.

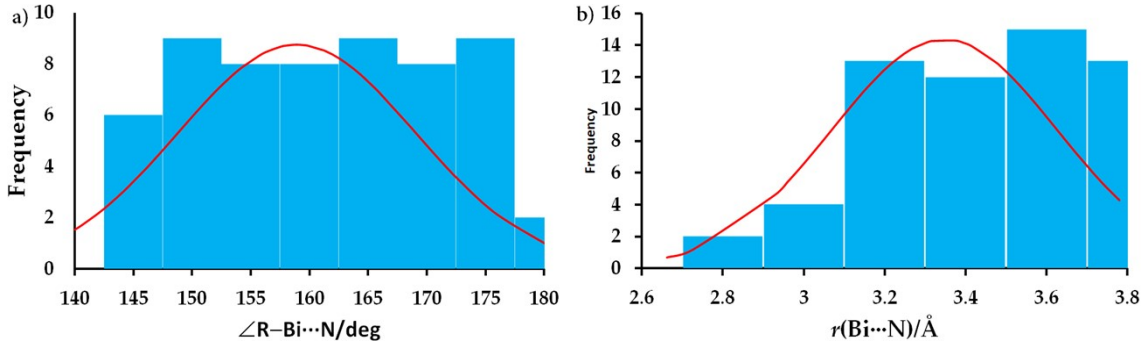

Figure S6. a) and b) Histograms showing, respectively, the angular and intermolecular distance distributions of 59 Bi···N close contacts in 40 crystals that emerged from a CSD search. The Bi···N intermolecular distance *r* (and intermolecular angle ∠R–Bi···N) in the range of 2.6–3.8 Å (140–180°) was used as a geometric criterion during the CSD search, where R represents any atom. Bond lengths and angles are shown in Å and degrees, respectively. The normal distribution curve is shown in dark-red in each plot.

The searches discussed above involved intermolecular distance less than the sum of the vdW radii of Bi and N, 4.20 Å. We performed a similar search with *r*(Bi···N) = 2.6 – 4.3 Å and ∠R–Bi···N = 140 – 180.0°. This gave 118 hits, with 214 close contacts (including false contacts). When the search did not involve any constraint, the number of hits and close contacts became 178 and 322, respectively. In these two cases, the peaks of the normal distributions, including false contacts, appeared around 3.73 Å and 155.5° for *r*(Bi···N) and ∠R–Bi···N, respectively.

D. Bi···X (X = F, Cl, Br, I) close contacts, with halogen derivatives as donors

Searches of the CSD for Bi···X (X = F, Cl, Br, I) were conducted with intermolecular distance *r* limited to ranges between 2.7 Å and an upper limit of (depending on the identity of X), 3.8, 4.3, 4.5 and 4.6 Å, respectively, and in all cases with the intermolecular angle ∠R–Bi···X limited to 140–180°. No close contacts were found below 2.7, 2.9, 3.2 and 3.4 Å for X = F, Cl, Br and I, respectively, which is unsurprising given the vdW radii of these elements increase with the increasing size of the halogen derivative (vdW radii values 1.46, 1.82, 1.86 and 2.04 Å, respectively[4]). The results are shown in Fig. S7. In all the four cases, the Bi···X intermolecular distances were found to range from either smaller to markedly greater than the sum of the vdW radii of Bi and X, emphasizing that a strict adherence to the use of the less than the sum of the vdW criterion to identify

non-covalent bonds would miss many genuine Bi···X close contacts in crystals, "a pitfall in the search for bonding".[11]

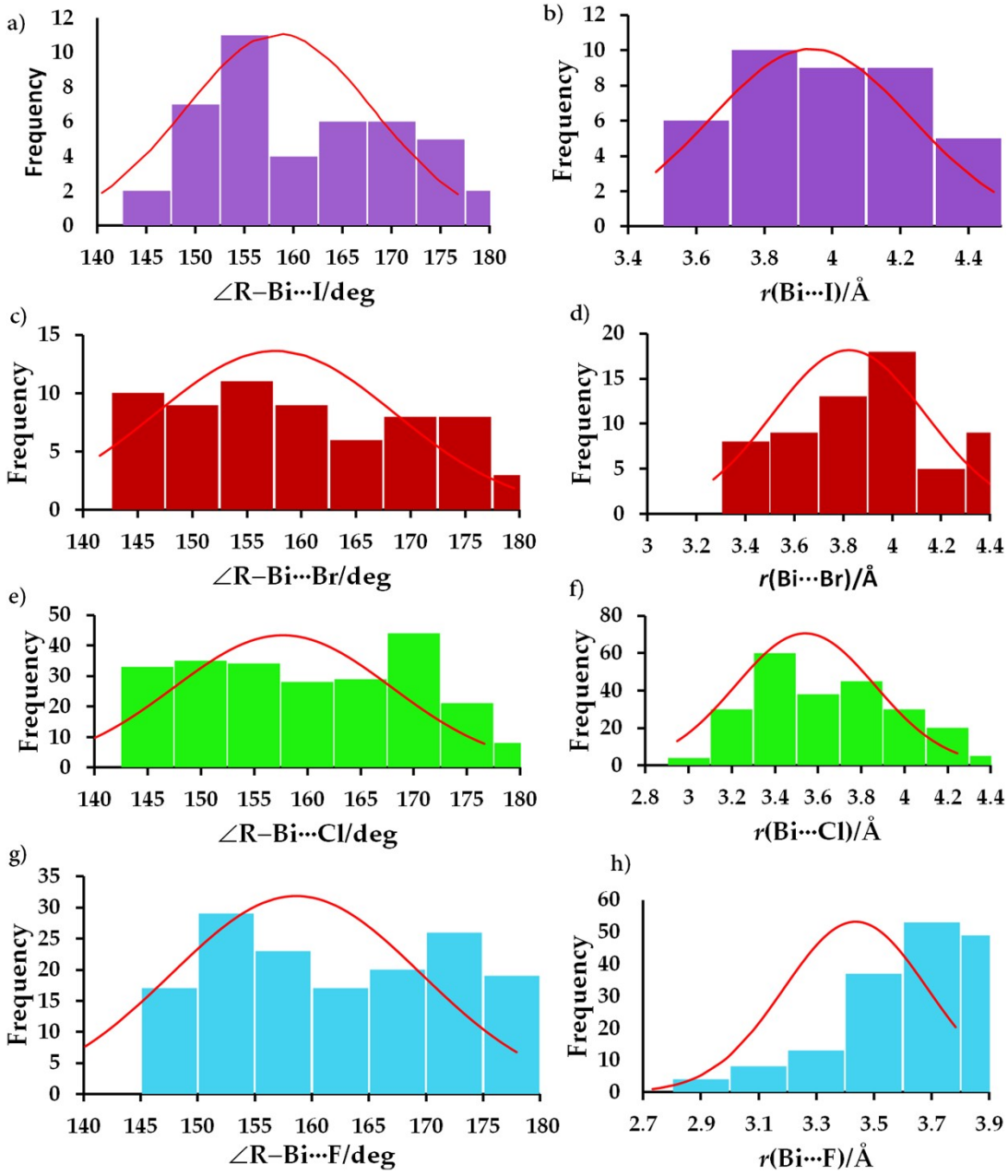

Figure S7. a) and b) Histograms showing, respectively, the angular and intermolecular distance distributions of 43 Bi···I close contacts in 30 crystals that emerged from a CSD search. c)-d), e)-f) and g)-h) are the corresponding plots for 64 Bi···Br close contacts in 41 crystals, 236 Bi···Cl close contacts in 136 crystals, and 168 Bi···Br close contacts in 89 crystals, respectively. The Bi···X (X = F, Cl, Br, I) intermolecular distance *r* (and intermolecular angle ∠R–Bi···X) in the ranges of 3.0–4.5 Å (140–180°), 2.8–4.5 Å (140–180°), 2.6–4.3 Å (140–180°) , and 2.6–3.8 Å (140–180°) was used as a geometric criterion during the CSD search for Bi···I, Bi···Br, Bi···Cl and Bi···F, respectively, where R represents any atom. Bond lengths and angles are shown in Å and degrees, respectively. The normal distribution curve is shown in dark-red in each plot.

From the histograms and normal distribution curves shown in Fig. S7a-h, it is clear that Bi···I, Bi···Br, Bi···Cl and Bi···F close contact distances occur approximately in the ranges 3.7 – 4.2, 3.6 – 4.1, 3.3 – 3.9 and 3.4 – 3.9 Å, respectively; each range is less than sum of the vdW radii of the respective atomic basins (r_{vdW}(Bi) + r_{vdW}(I) = 4.58 Å; r_{vdW}(Bi) + r_{vdW}(Br) = 4.40 Å; r_{vdW}(Bi) + r_{vdW}(Cl) = 4.36 Å; r_{vdW}(Bi) + r_{vdW}(F) = 4.0 Å). The upper limit of *r* used for each search was very close to the sum of the vdW radii sum of the appropriate atoms. We are cognizant that the vdW radii of atoms of the elements proposed separately by Batsanov[62] and Alvarez[4] are different, with r_{vdW}(Bi) = 2.3 and 2.54 Å, respectively. Note that an increase in the upper limit of the Bi···I contact distance from 4.5 Å to 4.8 (and 4.7) Å in the range 3.0–4.5 Å used in in the histogram in Fig. S7a, which is slightly longer than (r_{vdW}(Bi) + r_{vdW}(I) = 4.58 Å, did not give any additional crystals in our search of the CSD in the first case, and only increased the total number of Bi···I close contacts from 43 to 46. An un-constrained search with default *R*-factor gave 40 hits with 62 Bi···I close contacts. In the case of our search for Bi···Br with the change of criteria from (*r*(Bi···Br) [(∠R–Bi···Br)] = 2.8–4.5 Å [140–180°]) to (*r*(Bi···Br) [(∠R–Bi···Br)] = 2.8–4.7 Å [140–180°]), we found 64 Bi···Br close contacts in 41 crystals increased to 69 close contacts in 43 crystals.

It is clear from the plots in Fig. S7c and S7d that the number of Bi···Cl and Bi···F close contacts is greater than the number of Bi···I and Bi···Br close contacts in crystals. The peak of ∠R–Bi···X occurs between 150° and 165°, and there are a relatively very small number of such interactions that are linear. This is likely to be an effect of the involvement of other primary and/or secondary interactions associated with the electron density donors responsible for the formation of the bismuth bonds, as well as the ligating framework of covalently bound Bi.

E. Bi···π(arene) close contacts, with arene as donor

Given there is such an abundance of known π-systems, we limited our search of the Bi···π motif to cases where the π-density belongs to the centroid of a C_6 aromatic ring. Accordingly, and in our search, the Bi···C_6(centroid) distance and intermolecular angle ∠R–Bi···C_6(centroid) were constrained to the ranges of 2.8–4.5 Å and 140–180°, respectively. The search produced 216 crystals with 315 close contacts. Of these, eight crystals had nine false contacts that were rejected. We recognized them as false contacts since the positive site on covalently bound Bi in one molecular entity forms a bismuth bond with π-density on a single C atom (but not the centroid region) of the C_6 aromatic ring in another same or different molecular entity. For instance, this was observed in the crystal structures of tris(5-chloro-2-methoxyphenyl)-bismuth(III) (CSD ref. RAGBIO[63]), (μ_2-oxydiethan-2-yl)-tetraphenyl-di-bismuth (CSD ref: AVANOB[64]), and

bis(μ-chloro)-dichloro-bis(6-(diphenylphosphinoyl)-1,2-dihydroacenaphthylen-5-yl)-di-bismuth dichloromethane solvate (CSD ref. COJDIR[65]). The r(Bi···$C_\pi(C_6)$) [∠R–Bi···$C_\pi(C_6)$] in the corresponding systems were 3.619 Å [161.6°], 3.591 Å [173.8°], and 3.947 Å [160.1°], respectively. In other cases a genuine Bi···N contact was falsely detected as Bi···π(C_6), such as in tris(quinoline-8-thiolato)-bismuth (CSD ref: FUDMAS [66]).The false contacts show up in angular range 140–160°.

The normal distribution of the remaining close contacts in 208 crystals is shown in Fig. S8. The histogram in Fig. S8a shows that the population of ∠R–Bi··· C_6(centroid) is relatively low in the range 140 – 145°, and high in the range between 155 – 180°, with a peak of the bell curve occurring around 160°. Similarly, as may be readily seen from Fig. S8b, the population of the Bi···C_6(centroid) close contact distance is relatively less dense in the range 2.8 – 3.4 Å than in the range 3.5 – 4.5 Å, even though the peak of the bell curve appears at 3.86 Å.

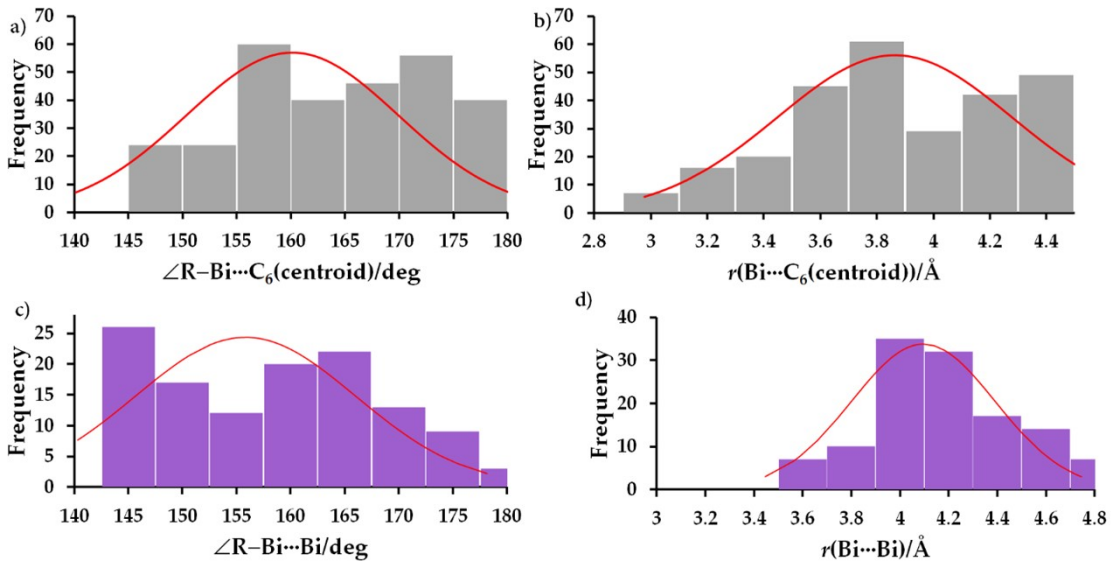

Figure S8. a) and b) Histograms showing, respectively, the angular and intermolecular distance distributions of 306 Bi···C_6(centroid) close contacts in 208 crystals originated from a CSD search. The Bi···C_6(centroid) intermolecular distance r (and intermolecular angle ∠R–Bi··· C_6(centroid) in the range of 2.6–4.5 Å (140–180°) was used as a geometric criterion during the CSD search, where R is any atom. c) and d) Histograms showing, respectively, the angular distribution and intermolecular distance of 12 Bi···Bi close contacts in several crystals originated from a CSD search (see text for discussion). Bond lengths and angles are shown in Å and degrees, respectively. The normal distribution curve is shown in dark-red in each plot.

F. Bi···Bi, and Bi···P close contacts, with pnictogen derivative as donor

A further search of Bi···Pn (X = P, As, Sb, Bi) intermolecular distance (and intermolecular angle ∠R–Bi···Pn) was individually carried out. These geometrical

constraints, limited to the range of 2.6–5.1 Å (140–180°), gave 383 crystals with 634 close contacts, where the upper limit of the distance range was very close to the sum of the vdW radius of Bi proposed by Alvarez, 5.1 Å ($\underline{r_{vdW}}$(Bi) = 2.54 Å).[4] A scrutiny of individual structures gave numerous false contacts probably because our search included both inter- and intra-molecular close contacts, and the angular flexibility was reasonably high. When the upper limit of the distance range was set equal to (or slightly larger than) the twice the vdW radius of Bi as proposed by Batsanov, 4.6 (4.8) Å ($\underline{r_{vdW}}$(Bi) = 2.3 Å),[62] our search of the CSD resulted in 224 (293) hits that comprised 373 (485) close contacts. When intramolecular close contacts were not included, our search resulted in 192 (258) crystal structures with 275 (373) close contacts. This suggests that the occurrence of Bi···Bi intramolecular close contacts in crystals is not very rare. Individual analysis of 293 crystals hits that comprised 485 close contacts led us to reject 363 close contacts out of a total of 485. The remaining 122 close contacts are shown in the histogram plot in Fig. S8c-d; there is no close contact in the range between 2.6 – 3.45 Å, except a single intramolecular interaction that exists between the Bi atoms in the crystal bis(μ-naphthalene-1,8-diyl)-diphenyl-di-bismuth ($C_{32}H_{22}Bi_2$, CSD ref. KARZEM[67]) that was reported this year; this was the shortest Type-III Bi···Bi close contact (*r*(Bi···Bi) = 3.227 Å and ∠R–Bi···Bi = 173.95°) among all close contacts identified. When the upper limit of (Bi···Bi) used in our search was set to 4.8 Å, a large number of close contacts subsequently identified to be false contacts arose. The criteria unequivocally detected Bi···Bi close contacts, even though the actual contacts in those crystals were Bi···O, Bi···S, Bi···N, Bi···C, Bi···C_π and Bi···X types, among others. An illustrative example is the crystal structure of the thioacyl bismuth complex (4-MeC_6H_4)Bi(4-$MeOC_4H_4COS)_2$ (CSD ref: ACUPEU[68]). This shows a purported Bi···Bi close contact of 4.370 Å, with a S–Bi···Bi contact angle of 177.3°. Yet visual inspection shows two other, probably more relevant, close contacts with Bi: Bi···O at 3.013 Å to one of the acyl O atoms of a neighboring entity, and of 3.429 Å to the O atom of a methoxy group of another. Clearly the purported Bi···Bi close contact is a false contact.

The results in Fig. S8c and d suggests that the population of bond distances and bond angles responsible for peaks in the normal distribution is around 155.8° and 4.1 Å, respectively. The strong population of bond angle around 145° suggests the Bi···Bi close contacts featuring this were secondary interactions, and are a consequence of primary interactions such as Bi···O, Bi···S, Bi···N, Bi···C, Bi···C_π, or Bi···X. The majority of the remaining 122 Bi···Bi close contacts were Type-III. *r*(Bi···Pn) and ∠R–Bi···Pn were in the ranges 3.5 – 4.7 Å and 145 – 175°, respectively. An example of the occurrence of a Type-III Bi···Bi close contact between the Bi$(CH_3)_3$ molecular units in crystalline

trimethylbismuthine (CSD ref: HUVQOG[69]) was readily apparent. In case of the crystals of Bi and Rh carbonyl anionic clusters (CSD ref: SOKVUM[70]) and Bi and Co anionic clusters (SOKWAT[70]), the Bi···Bi close contact occurs between the negative Bi sites of the interacting anions in the crystal.

A search of Bi···P inter- and intra-molecular distances (and inter- and intra-molecular angles ∠R–Bi···P) in the range of 2.6–4.5 Å (140–180°) gave 11 crystals with 23 close contacts. Of these, six crystals contained six false close contacts. These were found either between Bi in a cation and PF_6^- (as in $[C_{20}H_{21}BiCuN_4][PF_6]$ CSD ref: VEZCEL;[71] $[C_{48}H_{40}BiP_2[[PF_6]$, CSD ref: VISVUP;[72] and $[C_{20}H_{21}AgBiN_4][PF_6]$, CSD ref: VUGVOL,[73] or between ,Bi and P in a tert-butylphosphonato fragment (as in $C_{20}H_{39}BiN_2O_6P_2$, CSD ref. AQOLEY[74]).

The remaining 15 Bi···P close contacts were found in the crystals including tris(6-(diphenylphosphanyl)-1,2-dihydroacenaphthylen-5-yl)-bismuth(III) (CSD ref: GAJZOK[75]), (6-(di-isopropylphosphino)acenaphthylen-5-yl)-diphenyl-bismuth (CSD ref: OJAJIV[76]), bis(6-(di-isopropylphosphino)acenaphthylen-5-yl)-phenyl-bismuth (CSD ref. OJAJOB[76]), (bismuthinetriyltris(1,2-dihydroacenaphthylene-6,5-diyl))tris(di-isopropylphosphine) dichloromethane solvate (CSD ref: OTINIQ[77]) and tris(2-(diphenylphosphanyl)benzenethiolato)-bismuth (CSD ref: QEFVOO[78]). The intramolecular distances and angles in all these chemical systems were in the ranges 3.19 – 3.37 Å, and 140.6 – 173.4°, respectively, and none of the crystals featured intermolecular Bi···P close contacts. They all appear along the extension of the C–Bi covalent coordinate bonds, however. Whether or not the electrostatic potential on the surface of coordinate P in these systems is positive is not clear, and hence requires further theoretical exploration.

Searches of Bi···Sb and Bi···As in crystals in CSD with the same geometric criteria as above gave a few hits, but with false close contacts.

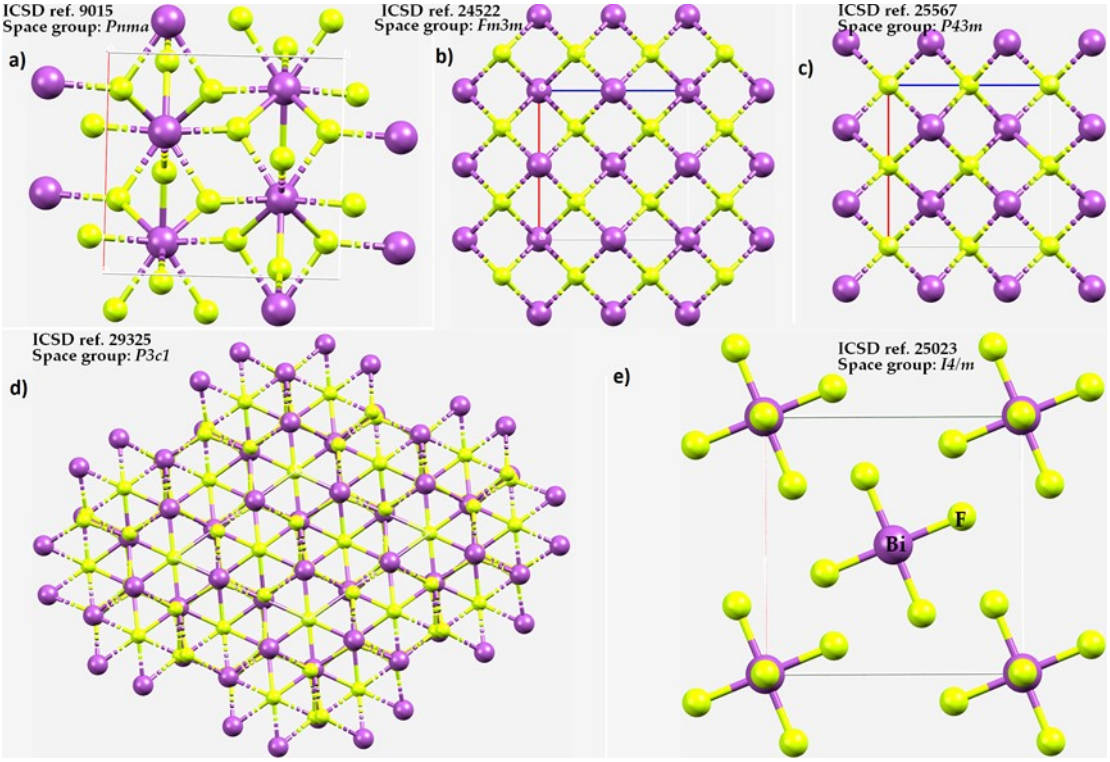

Figure S9. a)-d) Ball-and-stick models of the crystal structure of BiF_3 in different space groups; e) Ball-and-stick model of the crystal structure of BiF_5. The ICSD ref codes and space groups are shown for each case. Bonds are shown as sticks in atom color: Bi – purple; F – dark-yellow.

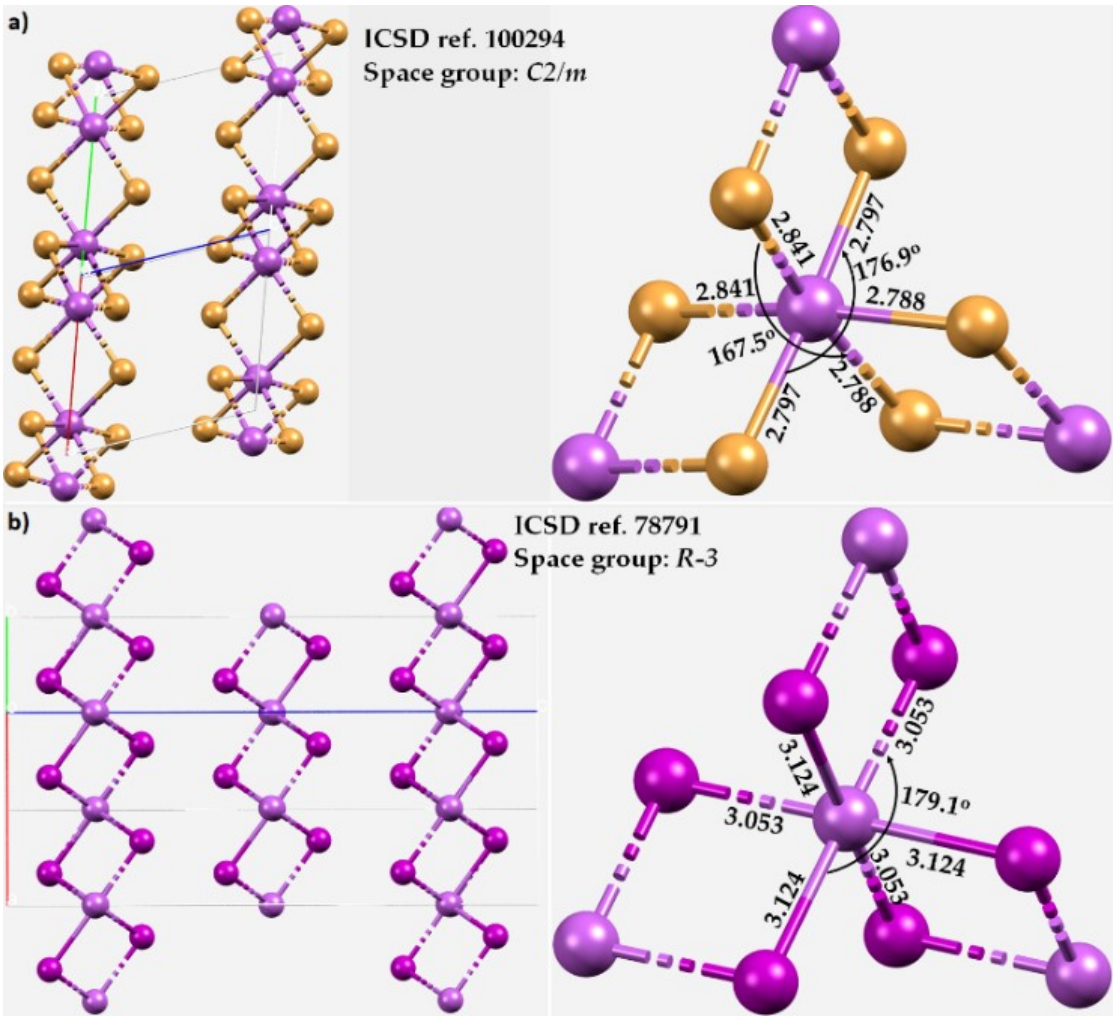

Figure S10. Ball-and-stick models of the crystal structures of a) $BiBr_3$ and b) BiI_3, showing layer-like structures in 2D. The ICSD ref codes and space groups are shown for each case. Selected bond distances and angles are in Å and degrees, respectively. Bonds are shown as sticks in atom color: Bi – faint-purple; I – purple; Br – faint-brown. Non-covalent interactions are shown as dotted lines in cyan.

S.F. The Physical Chemistry of Bi···O Pnictogen Bonds in Host-Guest Complexes

The boundary between coordinate (dative) and ordinary pnictogen bonds may be drawn with knowledge of the Bi···D bond distances. For instance, from Fig. 4a, it is apparent that the three Bi–Cl bond distances in $BiCl_3$ are nearly equivalent, with r(Bi–Cl) = 2.505, 2.503 and 2.539 Å. These are all less than 2.55 Å, and is true for all systems shown in Fig. 4 (except for Fig. 4c). On the other hand, the five Bi···O close contacts formed by the Bi center in $BiCl_3$ with the O-site of the crown ether are substantially longer, with r(Bi···O) = 2.871, 2.733, 3.008, 2.934, 3.221 and 2.871 Å. Given that the van der Waals radius of Cl (r_{vdW}(Cl) = 1.89 Å) is substantially longer than that of O (r_{vdW}(O) = 1.50 Å[4]), and that O is more electronegative, the Bi···O bond distances would have had to be much shorter to recognize these as coordinate bonds (as found for a Bi–O coordinate bond in the system in Fig. 4c). We therefore characterize the Bi···O close contacts in the μ_2-dibenzo-24-crown-8 system as strong pnictogen bonds rather than coordinate bonds. They are strong since the Bi···O bond distances are appreciably shorter than the sum of the vdW radii of Bi and O, 4.05 Å. This is also the case for the Bi···O close contacts in the host-guest complexes shown in Fig. 4b and 4d, but not that in Fig. 4c. In the latter, there is a single Bi···O close contact (r(Bi···O) = 2.490 Å) in the cation $(BiCl_2{\cdot}18\text{-crown-6})^+$ of the ionic compound $[2(BiCl_2{\cdot}18\text{-crown-6})^+.(Bi_2Cl_8)^{2-}]$ which is not only shorter than the two Bi–Cl coordinate bonds, but the remaining five Bi···O contacts are also close to the coordinate bond formation limit. The exception arises because of the $BiCl_2^+$ cation attracts the neutral ligand 18-crown-6 leading to the formation of a local cationic complex. In this sense, the bismuth cation is eight-coordinate involving all six oxygen atoms of the crown ether and two chloride ions in a bicapped trigonal prismatic geometry. These bonding features are markedly different from those observed for the crown ether complexes of BCl_3, $BiCl_3{\cdot}12\text{-crown-4}$ (Fig. 4d) and $BiCl_3{\cdot}15\text{-crown-5}$ (**Fig. 4b**) that are a neutral adducts with the pyramidal $BiCl_3$ linked to all four (five) oxygen atoms of the crown in a half-sandwich structure.

Another argument in support of our view on the formation of pnictogen bonds in the complexes shown in Fig. 4a,b,d is that all Bi···O close contacts are present along and off the extension of the C–Bi bonds in $BiCl_3$. This is because the electrostatic potential on Bi opposite the triangular face formed by the three chlorine atoms is completely positive (see Fig. 1b). These positive potential regions are capable of accepting electron density from the surrounding oxygen atoms of the crown ether. This is a perquisite to form a Type-II topology of the pnictogen bonding interaction (Scheme 1b).

We surveyed the Bi–O distances of crystals deposited in the CSD., We found 2559 contacts in 597 crystals in the range 1.8 to 4.5 Å. The peak of the normal distribution curve was at approximately 2.45 Å. There were no contacts below 2.013 Å or above 3.15 Å, indicating that all covalent, coordination, and strong pnictogen bonds are within this bond distance range. Considering that covalent and coordination bonds are generally stronger than pnictogen bonds, the best Bi–O coordination bonds in the crystal are expected to be around 2.6 Å, the boundary that tentatively separates Bi···O pnictogen bonds from the Bi–O coordinate bonds. When both Bi···O inter- and intramolecular close contacts were used as a search criterion and the bond between Bi and O was chosen to be of any type (single, double, and triple, etc), 5265 close distances were found in in 852 crystals. Of these, the Bi···O pnictogen bonds occurring between 3.15 and 4.50 Å could be considered having weak to moderate strength.

Our IGM-δg^{inter}-based results corresponding to the interactions between the bonded Pn site in $BiCl_3$ and the negative sites of the crown ether in Fig. 4a, 4b and 4d are shown in Fig. 11a, b and c, respectively. As we inferred from the intermolecular distances between Bi and O, we indeed observed IGM-δg^{inter} based isosurfaces between these atomic basins, indicative of genuine intermolecular bonding interactions. However, we found that there are two additional isosurfaces that show up between the Bi center in one $BiCl_3$ unit and the bonded Cl atom a neighboring molecule in the 12-crown-4 complex.[79] The Bi···Cl bond distance is 3.403 Å, and ∠Cl–Bi···Cl = 136.1° (see Fig. 4a). From the colors of the isosurfaces, and the bond distances, we conclude that those thick isosurfaces between Bi and ligating O atoms with a bluish color probably comprise some significant percentage of covalency and hence they may include some dative bond character. The remaining longer contacts are undoubtedly pnictogen bonds, and are quite evident in the crystal structure of the μ_2-dibenzo-24-crown-8 complex [80] shown in Fig. 4a and 5a.

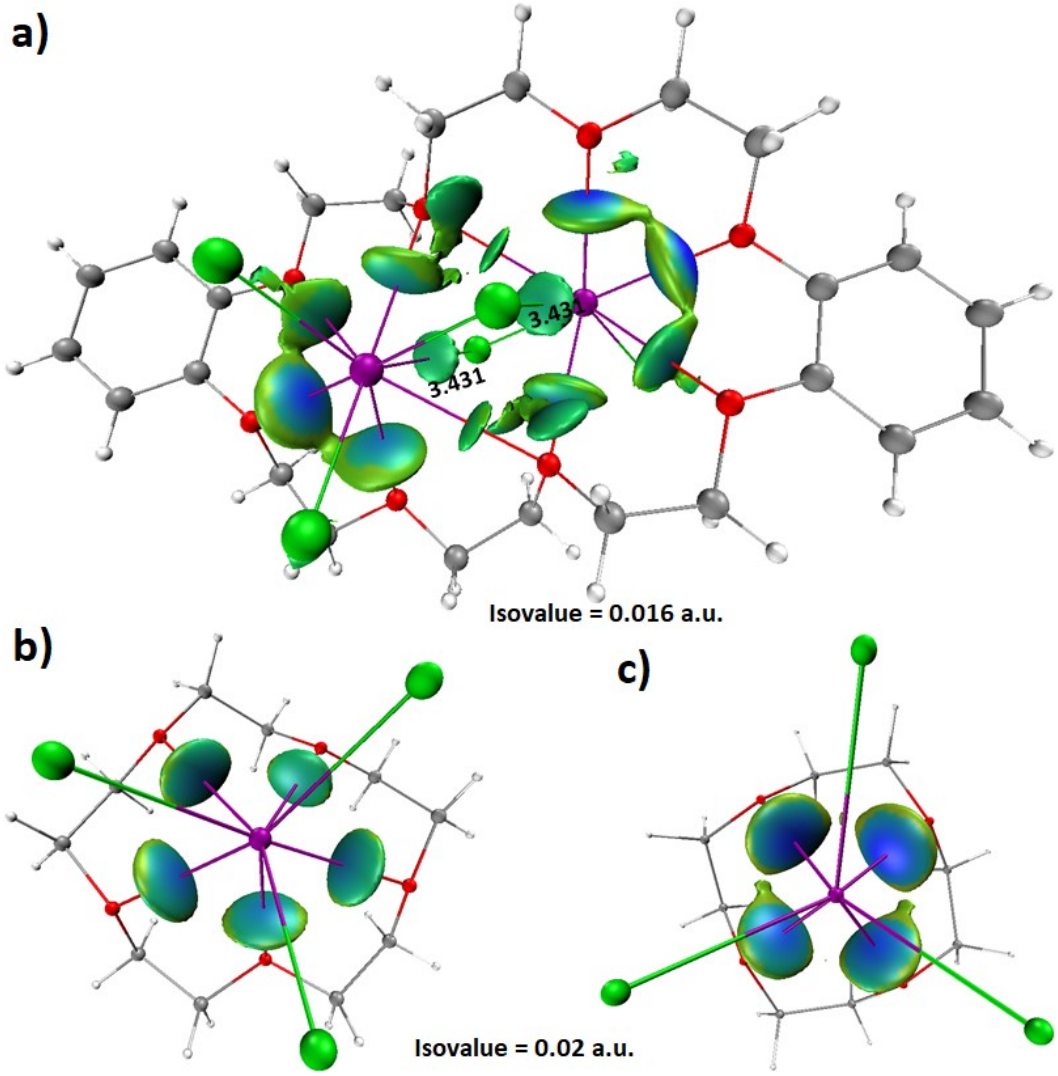

Figure S11. IGM-δg^{inter} based isosurface plots for the Bi^{3+} complexes with a) μ_2-dibenzo-24-crown-8;[80] b) 15-crown-5;[81] and c) 12-crown-4.[79] Isosurfaces colored blue and green indicate strong and medium-to-weak interactions, respectively. Isovalues used for the generation of isosurfaces are shown. Atom type and coloring is same as those shown in the ball-and-stick models in Fig. 4a, 4b and 4d, respectively. Selected bond lengths are in Å.

The crystal structure of the complex of BiI_3 and 15-crown-5[82] is shown in Fig. S12a. The bonding modes between Bi and O in the system are similar to those formed by the other members of the pnictogen trihalide family (*vide supra*). However, in the present case the Bi–I bonds are marginally longer than the Bi–O bonds. The former are formal coordinate bonds, expected of the BiI_3 molecule. The latter are comparable with that observed in the complexes of $BiCl_3$ with μ_2-dibenzo-24-crown-8[80] (Fig. 4a) and 15-crown-5[81] (Fig. 4b), and are pnictogen bonds given that they appear along and off the outer extension of the I–Bi bonds in BiI_3. One of the special features of this system is that the I sites of the Bi-coordinated crown ether are also engaged in forming long-ranged

I···I interactions that are directional in nature. The formation of both coordination bonds and I···I bonding interactions is in accord with the positive electrostatic potential on Bi and I along the I–Bi and Bi–I bond extensions (Fig. 1d); these are in attractive engagement with the negative lone-pair dominant sites on O and I, respectively. This also explains why the Bi–I···I angle deviates from linearity. The I···I halogen-halogen bonding interactions are responsible for the formation of the 1D chain-like architecture, Fig. 12a (left).

We used ωB97XD/def2-TZVPPD to energy minimize the geometry of the [BiI_3][15-crown-5] complex. This was done in the gas phase to gain a better understanding of the nature of the bonding interaction between BiI_3 and 15-crown-5 in the absence of crystal packing effects. The resulting fully relaxed geometry is shown in Fig. S12b. Two features are notable. First, all three Bi–I coordinate bond distances of BiI_3 are reproduced within 0.1 Å (Fig. S12a, right), while all the Bi···O bond distances between BiI_3 and 15-crown-5 are longer than found in the crystal (see Fig. S12a vs. Fig. S12b). The latter is expected since the effect of packing forces of the crystal lattice causes the Bi···O bond distances to shrink. Second, the three angles, ∠I–Bi···O, that appear along the extensions of the I–Bi bonds are all quasilinear (Fig. S12b), indicating the presence of σ-hole centered pnictogen bonds. Opposite to the triangular face formed by the three I atoms in BiI_3 (Fig. 1d), Bi is completely positive, so it is also linked to the remaining two O-sites of 15-crown-5. The latter two links are relatively long, with Bi···O bond distances of 3.226 and 3.346 Å, corresponding to bond angles of 138.1° and 134.7°, respectively. We designated the first three Bi···O links, which are along the extensions of the I–Bi bonds, as Type-IIa, and the latter two as Type-IIb pnictogen bonds; all are σ-hole centered.

The results of our QTAIM and IGM-δg^{inter} calculations performed on the wavefunction evaluated using the gas phase geometry of the complex of [BiI_3][15-crown-5] are shown in Fig. S12b and c, respectively. QTAIM has predicted the expected bond paths and bond critical points of charge density between Bi and O, as well as those between Bi and I. The charge density ρ_b at the Bi–I and Bi···O bond critical points (bcps) (0.0574 a.u. < ρ_b < 0.0580 a.u. and 0.0091 a.u. < ρ_b < 0.0161 a.u., respectively) are typical of non-covalent interactions, and the Laplacian of charge density $\nabla^2\rho_b$ values at the corresponding bcps are all small and positive (0.0412 a.u. < $\nabla^2\rho_b$ < 0.0438 a.u. at the Bi–I bcps, and 0.0272 a.u. < $\nabla^2\rho_b$ < 0.0498 a.u. at the Bi···O bcps), which indicate closed-shell (electrostatic) interactions. However, when the total energy density at the corresponding bcps was analyzed, it was found that H_b is negative for each of the three Bi–I coordinate bonds (–0.0140 < H_b < –0.0148 a.u.), and positive for Bi···O close contacts (0.0012 < H_b < 0.0014 a.u.). This provides further evidence that the former are genuine

(dative) coordinate bonds with appreciable covalent character, and the latter are (ordinary) pnictogen bonded interactions. These results are in agreement with IGM-δg^{inter} based isosurface charge density topologies (green volumes) between Bi in BiI_3 and the five ligating O sites in Benzo-15-crown-5, Fig. 6d. The ωB97XD/def2-TZVPPD level uncorrected and BSSE corrected binding energies of the complex calculated at the gas-phase geometry were –35.0 and –34.33 kcal mol^{-1}, respectively. The BSSE corrected stabilization energy of a single Bi···O pnictogen bond in [BiI_3][15-crown-5] complex is –6.86 kcal mol^{-1}; it is therefore a medium strength interaction,[83] and is certainly not a typical coordinate bond.

Very similar conclusions can be drawn from the structure of the [BiI_3][benzo-15-crown-5] complex, Fig. S12e. A coordination chemist would see this system as a neutral pseudo-octahedral complex, in which the [BiI_3][benzo-15-crown-5] units in the crystal are connected by secondary I···I halogen-halogen interactions forming chains in 1D.[84] The pseudo-octahedral nature of the system could be extracted based on the Bi–I and Bi···O bond distances (values between 2.8 and 3.0 Å), with the mean value of the former marginally longer than that of latter. By contrast, in the gas-phase structure, Fig. S12f, the order of the two types of bonding distances is reversed, i.e., r(Bi···O) > r(Bi–I). This is may be due to the absence of packing forces in the gas-phase structure, which allows the interacting molecules to bond freely without any constraints, which then permits the appearance of the genuine nature of the Bi···O and Bi–I interactions. Fiolka and coworkers[84] have claimed that the bonding between BiI_3 and benzo-15-crown-5 has to be mainly electrostatic as the interactions of the bismuth 6s lone pair with the 2p orbitals of the oxygen atoms of the crown ether are antibonding.

The bond path and bond critical point topologies of charge density, Fig. S12g, show the Bi–I and Bi···O links in [BiI_3][benzo-15-crown-5]. Their strengths are comparable with those found in [BiI_3][15-crown-5] (Fig. S12c), and are evidenced by the ρ_b values (0576 a.u. < ρ_b < 0.0586 a.u. at Bi–I bcps and 0.0108 a.u. < ρ_b < 0.0138 a.u. Bi···O). Given that 0.0423 a.u. (–0.0145 a.u.) < $\nabla^2\rho_b$ (H_b) < 0.0432 a.u. (–0.0150 a.u.) at the Bi–I bcps, and 0.0344 a.u. (–0.0013 a.u.) < $\nabla^2\rho_b$ (H_b) < 0.0433 a.u. (–0.0014 a.u.) at the Bi···O bcps, it may be concluded that the Bi–I bonds have both ionic and covalent character and the Bi···O links are largely electrostatically driven. Since the ωB97XD/def2-TZVPPD level uncorrected and BSSE corrected binding energies of the gas-phase geometry of the complex were –32.84 and –32.16 kcal mol^{-1}, respectively, the corrected energy of a single Bi···O pnictogen bond in the [BiI_3][benzo-15-crown-5] complex is –6.43 kcal mol^{-1}, meaning it is a medium strength interaction, and hence is not a typical (dative) coordinate bond. Provided the empirical relation, E_b = – ½V_b, is used, where E_b

represents the energy of a bond with potential energy density V_b at bcp, the energies of all the five Bi···O close contacts lie between – 3.7 and –5.2 kcal mol^{-1}, which supports the view that the Bi···O interactions have the characteristic of medium strength (ordinary) pnictogen bonds.

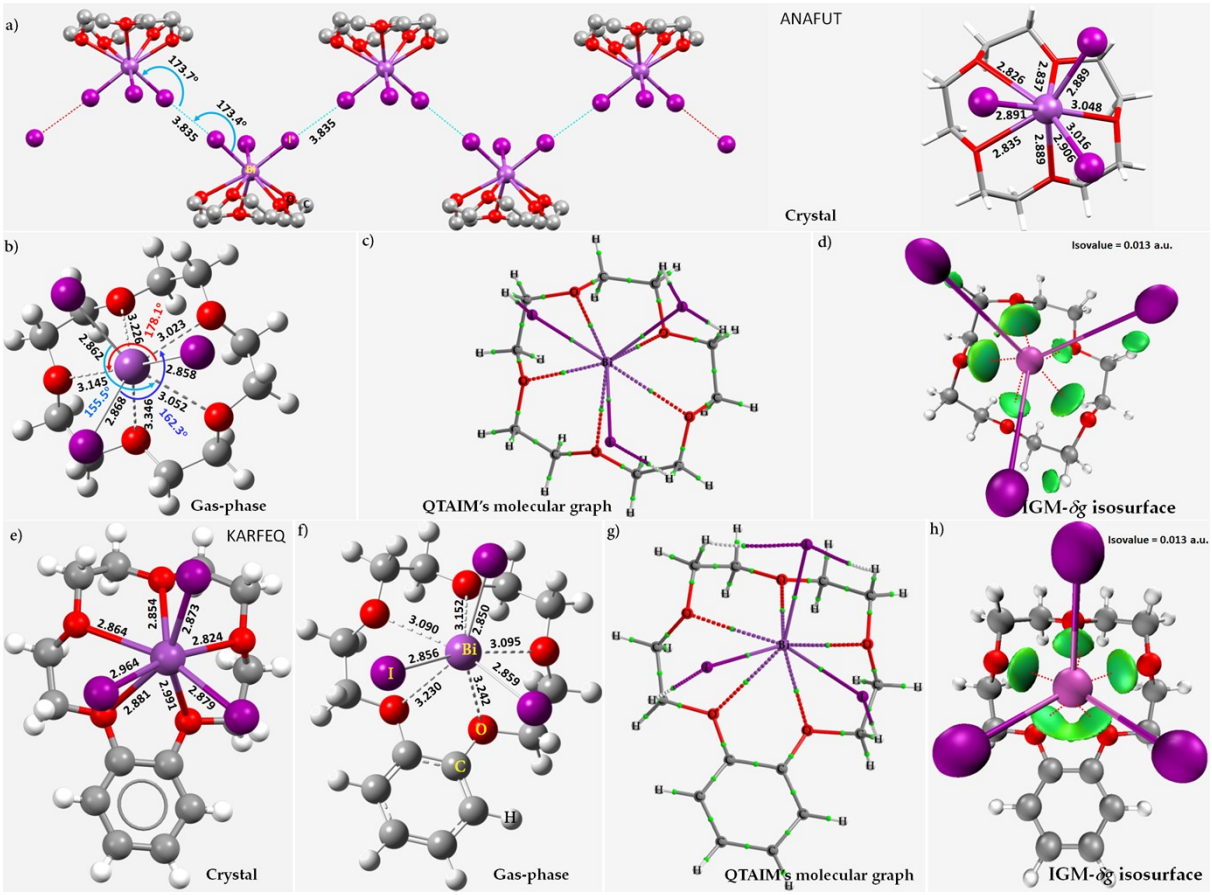

Figure S12. Nature of intermolecular bonding in the crystal structure of [BiI_3][15-crown-5] (CSD ref code AMAFUT);[82] H atoms are omitted from figure on left; the I···I contacts are shown as dotted lines in cyan. b), c) and d) Gas-phase fully-relaxed geometry, QTAIM-based molecular graph and IGM-δg^{inter} based isosurface charge density topologies between Bi in BiI_3 and O donors in 15-crown-5, respectively, obtained using ωB97XD/def2-TZVPPD. e), f), g) and h) The crystal geometry, gas-phase fully-relaxed geometry, QTAIM-based molecular graph, and IGM-δg^{inter} based isosurface charge density topologies between Bi in BiI_3 and donors in benzo-15-crown-5, respectively, with the latter three obtained using ωB97XD/def2-TZVPPD. Bond paths as sticks and dotted lines in atom color between bonded atomic basins, and bond critical points between bonded atomic basins as tiny spheres in green in c) and g) are shown. Selected bond lengths (Å) and bond angles (degrees) are depicted. The CSD references for the crystals are shown in a) and e) in uppercase letters.

S.G Bi···O, Bi···P, Bi···S, Bi···N, Bi···C_π, Bi···Se, and Bi···X (X = Cl, Br, I) Pnictogen Bonds in a Variety of Crystals

Breunig and Althaus reported a number of alkylantimony(III) and alkylbismuth(III) halides, R_2EX and REX_2, (E = Sb, Bi; X = Cl, Br, I; R = CH_3, $(Me_3Si)_2CH$) and demonstrated that they form oligomeric or polymeric structures through halogen bridges between the pnictogen atoms.[85] Bi^{3+} in these compounds is genuinely five-coordinate. In the complex with CH_3BiBr_2 and with THF solvate in the crystal structure (Fig. S13a), in addition to binding to the methyl and bromide ligands, Bi^{3+} is coordinated by lone pairs on oxygen from two THF solvent molecules.

The possibility of pnictogen bonding in either of the R_2EX and REX_2 systems was not discussed in the original study.[85] However, as noted just above, the authors suggested the existence of halogen bridges between the covalently bound pnictogen atoms and the halide. To verify this, we performed a pro-molecular IGM-δg^{inter} analysis on a dimer $CH_3BiBr_2.2THF$. The result, shown in Fig. S13b, suggests that one monomer is linked to the other through a Type-IIa $(H_3)C$–Bi···Br(Bi) pnictogen bond, but this has nothing to do with halogen bridges. The presence of the pnictogen bond is evidenced by the greenish isosurface between the Br and Bi atomic basins. We classify them as pnictogen bridges; there are two such equivalent pnictogen bridges, each with r(Bi···Br) = 3.979 Å and ∠(CH_3)C–Bi···Br = 167.5°, and are markedly longer than the Bi–O (= 2.60 Å), Bi–C (= 2.25 Å) and Bi–Br (= 2.70 Å) coordinate bonds of the complex.

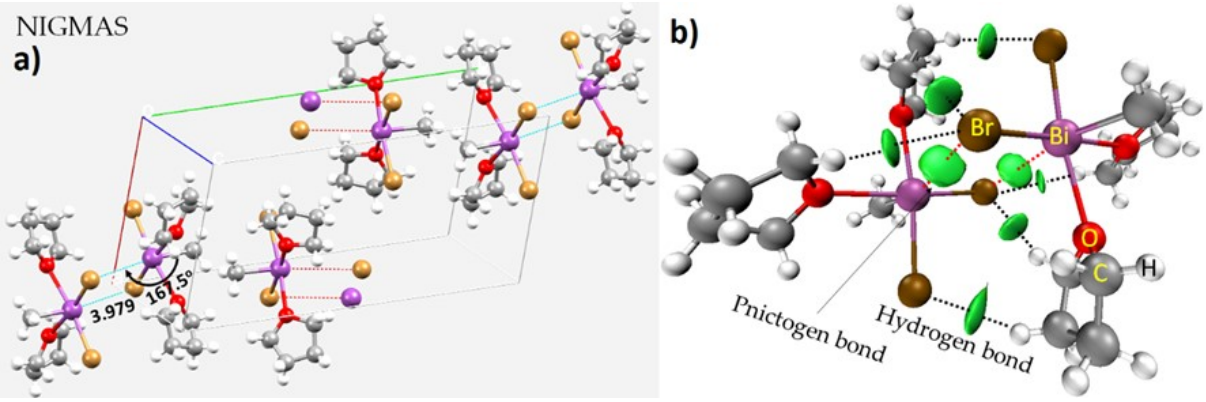

Figure S13. a) The crystal structure of $CH_3BiBr_2.THF$, CSD ref. code NIGMAS.[85] b) The IGM-δg^{inter} based isosurface topologies (isovalue = 0.01 a.u.) of bonding observed between bonded atomic basins in the dimer $[CH_3BiBr_2.2THF]_2$. Selected bond lengths and bond angles are in Å and degrees, respectively. Non-covalent interactions are shown as dotted lines.

The formation of these pnictogen bridges is not very surprising given that the Bi site along the $(H_3)C–Bi$ bond in a molecular entity features a positive σ-hole and is engaged with the lateral negative portion of the covalently bound Br atom in a neighboring molecular entity. The $(H_3)C–Bi\cdots Br(Bi)$ pnictogen bonds are somewhat deviated from linearity, which is understandable since Br in each molecular entity also participates in $Br\cdots H(CH)$ hydrogen bonded with THF (see Fig. S13b). Clearly, the packing between the molecules in the crystal is a consequence of the joint involvement of pnictogen bonds and hydrogen bonds. It is worth nothing that Bi is four-coordinate in the sterically crowded crystal of $(Me_3Si)_2CH)$ $BiCl_2$.THF (CSD ref: DABWOT).[85] The Bi center in this system was bonded to the Cl site in a neighboring molecule in the crystal, forming two equivalent $Bi\cdots Cl$ long bonds ($r(Bi\cdots Cl) = 3.163$ Å; $Cl–Bi\cdots Cl = 160.4^o$) with the characteristics of Type-IIa pnictogen bonds.

Shown in Fig. S14a-h are a set of crystals in which covalently or coordinately bound Bi is in attractive engagement with donors such as O, N, Cl, S, and I in interacting partner spices. Except for the crystals $2(C_{10}H_{12}S_8^+)(Bi_3Cl_{11}^{2-})$[86] and $(C_{12}H_{10}BiI_2^-)(C_8H_{20}N^+)$[87] shown in Fig. S14d and 1g, respectively, the Bi center in the remaining crystals is positive. Although a Type-IIa bonding featuring Bi is occurs in all eight crystals of Fig. 14, this is not the case in the structures shown in Fig. S14d and g because Bi is entirely negative in these two crystals. This means that the appearance and subsequent stability of the $Bi\cdots Cl$ and $Bi\cdots I$ directional interactions in the respective crystals are driven by the cation, and hence may characterized as Type-III interactions. On the other hand, the $Bi\cdots I/Bi\cdots C_\pi$, $Bi\cdots O$, $Bi\cdots N/C\equiv N$, $Bi\cdots Se$, $Bi\cdots\pi(C_6)$ and $Bi\cdots Cl$ in the crystals shown in Fig. 14a, b, c, e, f and h, respectively, have the characteristics of pnictogen bonds since they appear along R–Bi bond extensions, and are less than the sum of the vdW radii of the respective interacting atomic basins.

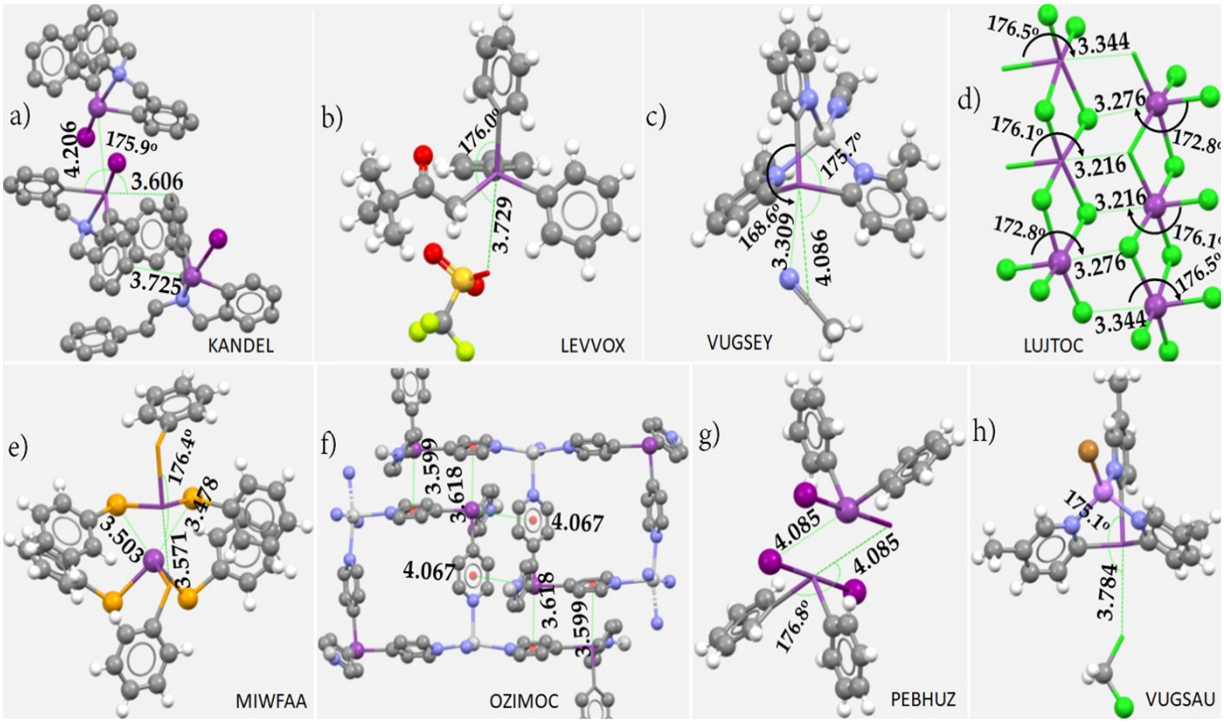

Figure S14. Crystal structures showing close contacts of covalently or coordinately bound Bi with O, N, Cl, Se, C_π and I sites in interacting partner spices: a) (2,2'-[[(2-phenylethyl)azanediyl]bis(methylene)]di(benzen-1-yl))-iodo-bismuth(III) ($C_{22}H_{21}BiIN$);[39] b) (3,3-dimethyl-2-oxobutyl)-triphenyl-bismuth trifluoromethanesulfonate ($C_{24}H_{26}BiO^+$)($CF_3O_3S^-$);[88] c) acetonitrile-[2,2',2''-bismuthanetriyltris(6-methylpyridine)]-silver trifluoromethanesulfonate acetonitrile solvate ($C_{20}H_{21}AgBiN_4^+$)($CF_3O_3S^-$)(C_2H_3N);[73] d) bis(tetrakis(methylthio)tetrathiafulvalene radical cation) tetrakis(μ-chloro)-heptachloro-tri-bismuth(III) 2($C_{10}H_{12}S_8^+$),($Bi_3Cl_{11}^{2-}$) [86]; e) tris(phenylselenolato)-bismuth ($C_{18}H_{15}BiSe_3$);[89] f) catena-[nonakis(μ-pyridin-4-yl)-tri-bismuth(III)-di-silver(I) bis(hexafluoroantimonate) [($C_{45}H_{36}Ag_2Bi_3N_9^{2+}$)$_n$,2($SbF_6^-$)];[90] g) tetraethylammonium di-iodo-diphenyl-bismuth ($C_{12}H_{10}BiI_2^-$)($C_8H_{20}N^+$);[87] h) [2,2',2''-bismuthanetriyltris(5-methylpyridine)]-bromido-lithium dichloromethane solvate ($C_{18}H_{18}BiBrLiN_3$)(CH_2Cl_2).[73]Selected bond lengths and bond angles are in Å and degrees, respectively. Non-covalent interactions are shown as dotted lines. H atoms in a) are omitted for clarity. The tiny dot at the center of the aromatic ring in f) represents the centroid.

In the crystals shown in Fig. 15a-g, the covalently or coordinately bound Bi is positive along the R–Bi bond extensions, except for the building block $Bi_4I_{16}^{4-}$ in ($C_{24}H_{20}Bi^+$)$_4$($Bi_4I_{16}^{4-}$).[53] The ∠R–Bi···D (D = N, O, Cl, and C_π) between the interacting units in these crystals lie between 175° and 180°, regardless of the electron density donors concerned. In all cases, the Bi···D pnictogen bond distances are less than the sum of the vdW radii of the respective atomic basins. They follow a Type-IIa topology of bonding (Scheme 1). In case of (2-((dimethylamino)methyl)phenyl)-diphenyl-bismuth ($C_{21}H_{22}BiN$), (Fig. 15e),[91] the N of the dimethylamino group pnictogen bonds with Bi forming a Bi···N intra-molecular contact (r(Bi···N) = 2.851 Å; ∠C–Bi···N = 161.9°) (not

shown), which is markedly longer than Bi–C coordinate bonds (r(Bi–C) between 2.255–2.295 Å) but significantly shorter than the Bi···C_π pnictogen bond (r(Bi···C_π) = 3.859 Å).

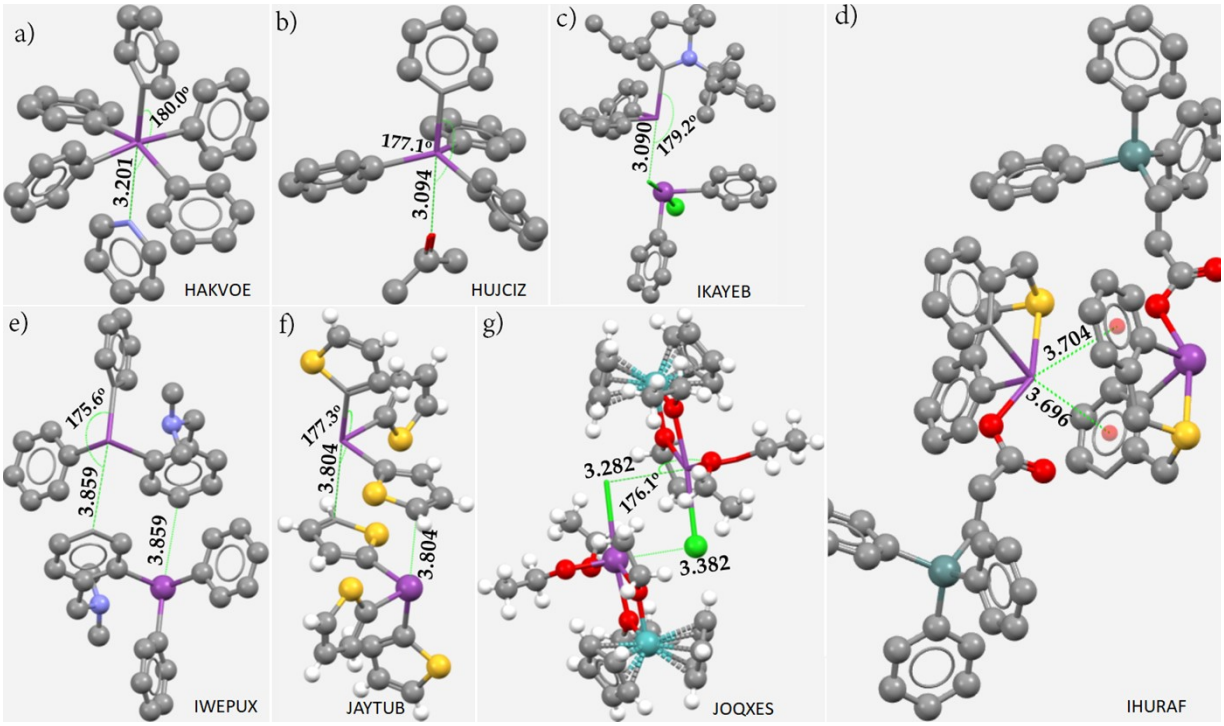

Figure S15. Some crystal structures showing close contacts of covalently or coordinately bound Bi with O, N, Cl, and C_π sites in interacting partner species. a) pentaphenyl-bismuth pyridine solvate, $C_{30}H_{25}Bi)C_5H_5N)$;[92] b) tetrakis(tetraphenyl-bismuth) bis(μ_3-iodo)-tetrakis(μ_2-iodo)-decaiodo-tetra-bismuth acetone solvate $(C_{24}H_{20}Bi^+)_4(Bi_4I_{16}^{4-})2(C_3H_6O)]$[53] c) (1-[2,6-bis(propan-2-yl)phenyl]-3,3-diethyl-5,5-dimethylpyrrolidin-2-ylidene)-diphenyl-bismuth(III) dichloro-diphenyl-bismuth(III) $(C_{34}H_{45}BiN^+)(C_{12}H_{10}BiCl_2^-)$;[93] d) (bis(o-phenylenemethylene)thioxy)-(3-triphenylgermylpropionato)-bismuth(III) $[C_{35}H_{31}BiGeO_2S]$;[94] e) (2-((dimethylamino)methyl)phenyl)-diphenyl-bismuth ($C_{21}H_{22}BiN$) [91]; f) tris(thiophen-2-yl)bismuthane ($C_{12}H_9BiS_3$) [95]; g) bis(μ_2-ethoxo)-chloro-bis(η^5-cyclopentadienyl)-bis(ethanolato)-bismuth-molybdenum ethanol solvate $(C_{18}H_{30}BiClMoO_4)0.25(C_2H_6O)$.[96] Selected bond lengths and bond angles are in Å and degrees, respectively. Non-covalent interactions are shown as dotted lines. H atoms in a)-e) and (C_2H_6O) in g) are omitted for clarity. The tiny dot at the center of the aromatic ring in d) represents the centroid.

As shown in several cases above, pnictogen derivatives in molecules can form neutral or anionic square pyramidal structures. Shown in Fig. S16 is another such instance, in which the Bi center in the 1 × 2 × 1 extended crystal structure of $[CH_3BiCl_2(bipy)]$[97] adopts a square-pyramidal geometry. This crystal system provides evidence of pnictogen bonding between the covalently/coordinately bound Bi^{3+} in one molecule and coordinated Cl^- in a neighboring molecule. The C–Bi···Cl pnictogen bonding interaction is at 3.638 Å with ∠C–Bi···Cl = 158.9°, displaying therefore a Type-

IIa bonding topology. The stability of the crystal arises not only from pnictogen bonding, but also from significant π···π stacking interactions existing between the aromatic rings of the bipy units and from Cl···H(bipy) hydrogen bonds (not shown).

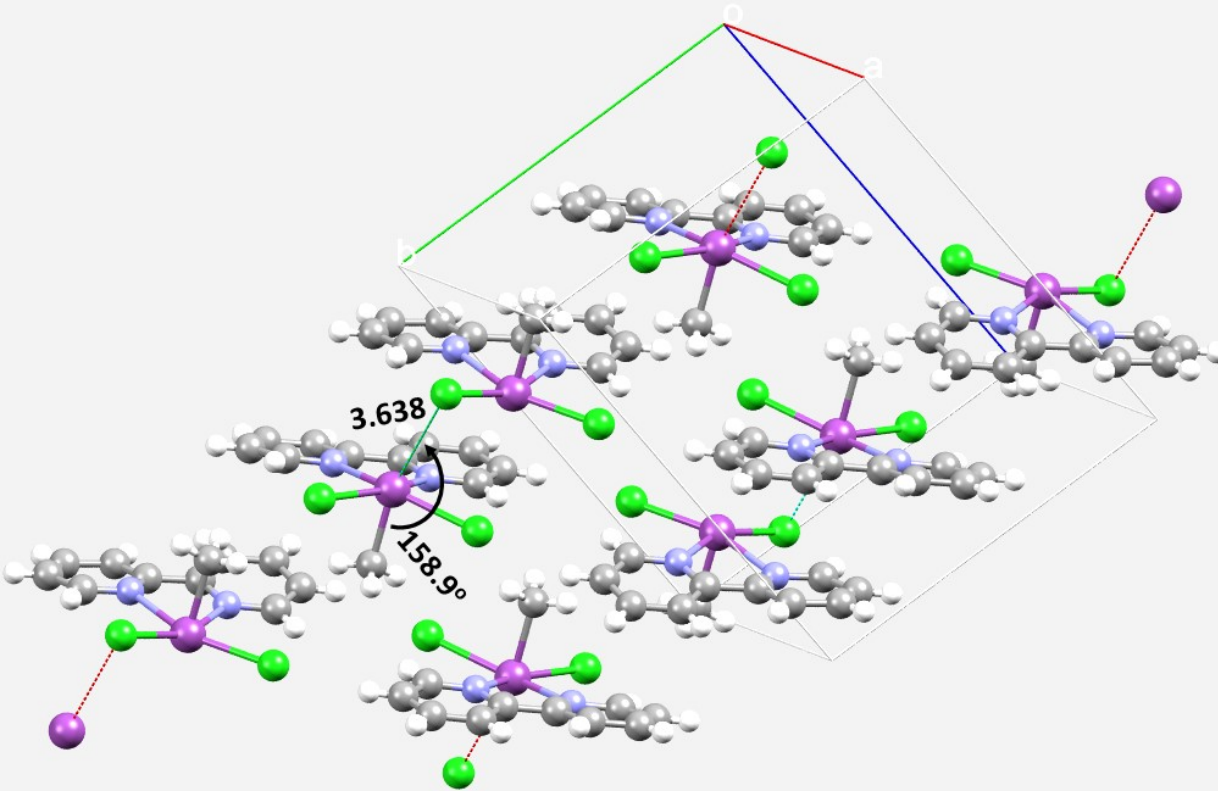

Figure S16. The ball-and-stick model of the crystal structure of [CH_3BiCl_2(bipy)] (bipy = 2,2′-bipyridyl), CSD ref. code EDIGED, space group *P*–1.[97] Selected bond lengths and bond angles are in Å and degrees, respectively. Atoms: Bi – purple; Cl – green; C – gray; N – blue; H – white.

S.H Type-III Pnictogen Bonds in Crystals

To confirm that a Bi···Bi Type-III bond exists between a pair of molecular entities shown in Fig. 8, we examined the MESP plot of trimethylbismuthine, shown in Fig. S17a-b. This was obtained on the fully relaxed monomer geometry of the system with *ω*B97XD/def2-TZVPPD. As can be seen from Fig. S17a, there are three σ-holes on Bi along the C–Bi bond extensions, each associated with a $V_{S,max}$ = 16.2 kcal mol^{-1}. The lateral side of Bi, which is facing the reader, is very negative, with $V_{S,min}$ = –6.3 kcal mol^{-1}. The carbons of the methyl groups attached to Bi are all negative and H atoms are all positive along the Bi–C and C–H bond extensions, respectively. The opposite side of Bi (Fig. S17b), also shown facing the reader, is positive. Clearly, Bi in $Bi(CH_3)_3$ has both positive and negative regions, and can react with another identical or different system both as an acid and a base. The quasilinear Bi···Bi bonding that exists between the Bi

atoms in Fig. 8f is a result of attraction between two positive sites of unequal charge density located along and slightly off the C–Bi bond axes in $Bi(CH_3)_3$. This is readily appreciated by looking at the space-filling model of the $(Bi(CH_3)_3)_2$ dimer arrangement (Fig. S17c) extracted from the crystal of the system shown in Fig. 15d. It is also possible that there are some attractive interactions existing between Bi and C domains that might simultaneously cause the formation of weakly bound Bi···C pnictogen bonds.

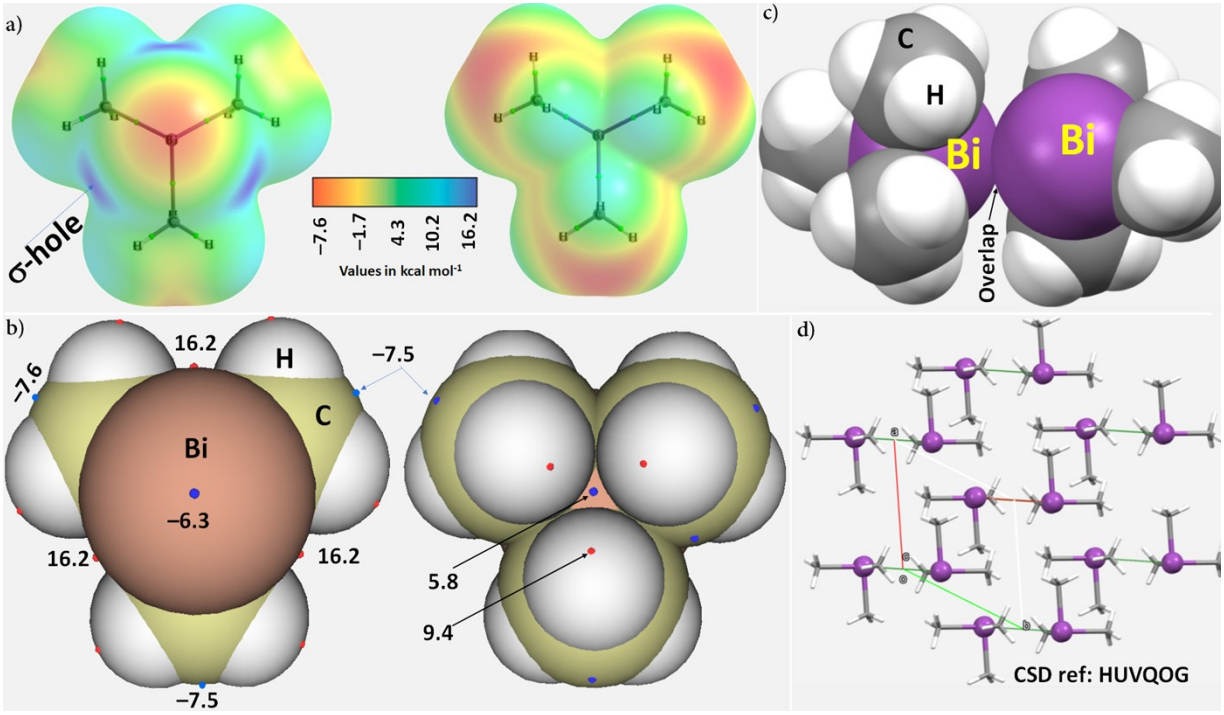

Figure S17. a) Two views of the 0.001 a.u. isoelectron density envelope mapped potential on the surface of the $Bi(CH_3)_3$ molecule, obtained using its *ω*B97XD/def2-TZVPPD geometry at the same level: (left) Bi facing the reader; (right) Opposite site of Bi facing the reader. b) Two views of the van der Waals surface of the corresponding same system, with the minimum and maximum of potential as tiny circles in blue and green, respectively. c) The space-filling model representing the extent of overlap between the two interacting Bi atoms of two nearest $Bi(CH_3)_3$ molecules in the crystal. d) The 2 × 2 × 2 representation of the $Bi(CH_3)_3$ crystal, with the Bi···Bi links as dots in cyan. The CSD ref. code is shown in upper case letters in d).

S.I. Intramolecular Pnictogen Bonds

The reaction of $(C_6F_5)_2GeH_2$ with $BiEt_3$ produces $[(C_6F_5)_2Ge]_3Bi_2$.[98] It features a trigonal bipyramid in which the two apical Bi atoms are linked covalently with three bis(pentafluorophenyl)germyl bridges. The molecular framework has D_{3h} symmetry, and is shown in Fig. S18a.

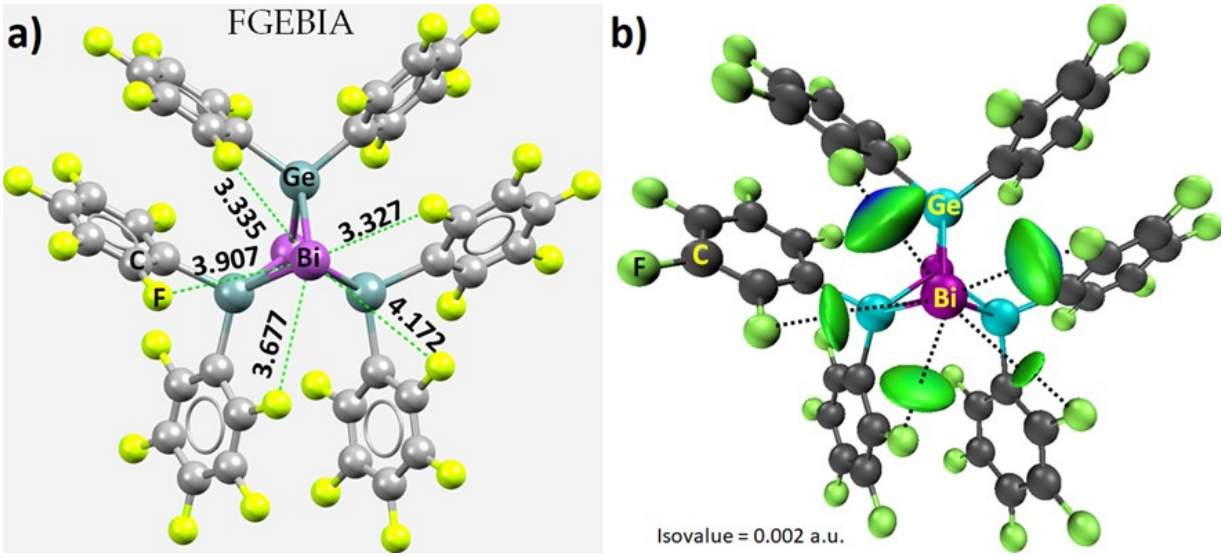

Figure S18. a) The tris(μ_2-bis(pentafluorophenyl)-germyl)-di-bismuth molecule, $[(C_6F_5)_2Ge]_3Bi_2$, found in the a heteroelemental crystalline network (CSD ref. FGEBIA[98]), showing a number of intramolecular Bi···F interactions. b) The IGM-δg^{inter} based isosurface plot. Selected bond lengths are in Å. Non-covalent interactions are shown as dotted lines between bonded atomic basins.

The average Ge–Bi bond length is 2.739(1) Å and the Bi···Bi distance is 4.005 Å, with the latter substantially smaller than twice the vdW radius of a Bi atom, 5.08 Å. There are additional intramolecular interactions within the framework of $[(C_6F_5)_2Ge]_3Bi_2$. Each apical Bi bonds non-covalently with the five nearest F atoms of the three bis(pentafluorophenyl) moieties. This became evident on exploring the system with an IGM-δg^{inter} based isosurface analysis (Fig. S18b). Although the very long Bi···F interaction (r(Bi···F) = 4.172 Å) was evident only when a very small isosurface value of 0.003 a.u. was used in the analysis, the two that are described by the thick greenish-blue volumes between the Bi and F atomic basins were always present regardless of the isovalue used. These two interactions are stronger than the remaining three Bi···F interactions which fall into the weak-to-vdW regime. These results demonstrate that Bi has the capacity to form at least five intramolecular interactions that are a characteristic of non-linear Type-IIb pnictogen bonds in addition to the three formal Bi–Ge ionic bonds.

The molecular structures of two hybrid dibismuthines, ($O[(CH_2)_2BiPh_2]_2$) and ($S(CH_2\text{-}2\text{-}C_6H_4BiPh_2)_2$) that form crystalline materials are shown in Fig. S19a and b (left) of , respectively.[64]. In these two systems, intramolecular interactions dominate within the molecular frameworks which we assign as C–Bi···O and C–Bi···S intramolecular pnictogen bonds, respectively. The latter are comparable to the C–Sb···S interaction observed in an analogous crystal system, ($[S(CH_2\text{-}2\text{-}C_6H_4SbMe_3)_2]I_2$) (Fig. S19c, left). They are the result of attractive engagements between the positive site on the electrostatic surfaces of the Bi/Sb atoms along the C–Bi/C–Sb bond extensions and negative sites localized on the O/S atom. As such, each molecular framework comprises of two intramolecular interactions. They are nearly equivalent in $O[(CH_2)_2BiPh_2]_2$ and $S(CH_2\text{-}2\text{-}C_6H_4BiPh_2)_2$, and significantly non-equivalent in $[S(CH_2\text{-}2\text{-}C_6H_4SbMe_3)_2]^{2+}$. This conclusion is arrived at based on the observed differences in the two (C–)Bi···O/(C–)Bi···S/(C–)Sb···S bond distances in $O[(CH_2)_2BiPh_2]_2$ or $S(CH_2\text{-}2\text{-}C_6H_4BiPh_2)_2$, or $[S(CH_2\text{-}2\text{-}C_6H_4SbMe_3)_2]^{2+}$. For instance, in the latter system, the (C–)Sb···S bond distances are very different, 3.555 and 4.419 Å (Fig. S19c), whereas the (C–)Bi···O bond distances in Fig. S19a are 3.203 and 3.126 Å, and (C–)Bi···S bond distances in Fig. S19b are 3.301 and 3.325 Å. Moreover, the long and short C–Bi···O pnictogen bonds in $O[(CH_2)_2BiPh_2]_2$ have ∠C–B···O values of 140.5° and 142.8°, respectively. These are Type-IIb interactions and non-linear pnictogen bonds. For $S(CH_2\text{-}2\text{-}C_6H_4BiPh_2)_2$, the corresponding angles associated with the short and long bonds are 161.4° and 163.1°, respectively, which are clearly Type-IIa interactions. However, in $[S(CH_2\text{-}2\text{-}C_6H_4SbMe_3)_2]^{2+}$, the ∠C–Sb···S associated with the short and long bonds are 169.8° and 125.9°, respectively, suggesting the former is a Type-IIa and the latter a Type-IIb interaction. Since the development of both these interactions occur with the same dicationic molecule – one quasi-linear and one non-linear – the former and latter may fall into the Type-III and Type-Ib category of pnictogen bonding (as there is no involvement of a negative site on the S in making the Sb···S bonds).

The characterization of (C–)Bi···O/(C–)Bi···S/(C–)Sb···S pnictogen bonding interactions in the three systems discussed above and based on the nature of the bond distances and bond angles is confirmed by the IGM-δg^{inter} based isosurface plots shown in Fig. S19a-c (right). The isosurface between Sb and S atomic basins appears at a very small isovalue of 0.003 a.u., suggesting that this interaction is of the vdW type.

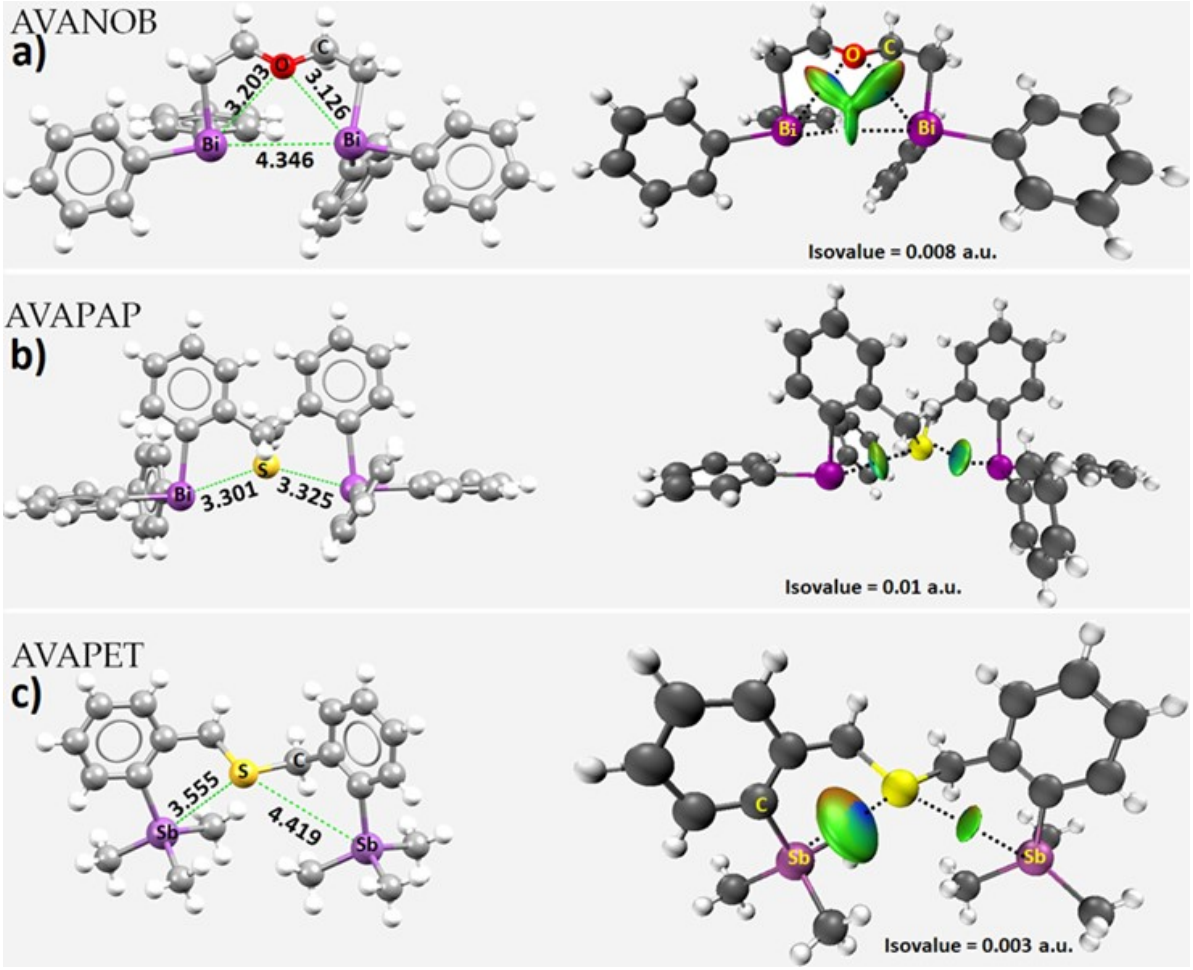

Figure S19. a)-c) (Left) Ball-and-stick models of the structure of some molecules displaying the involvement of Bi/Sb in intramolecular interactions;[64] (Right) The corresponding IGM-δg based isosurface plots. The crystalline materials are a) (μ_2-oxydiethan-2-yl)-tetraphenyl-di-bismuth; b) (μ_2-2,2'-(2-thiapropan-1,3-diyl)diphenyl)-tetraphenyl-di-bismuth; c) (μ_2-2,2'-(2-thiapropan-1,3-diyl)diphenyl)-hexamethyl-di-antimony bis(iodide). Bond lengths are shown in Å, and the dication in c) is stabilized with the assistance of two iodide anions (not shown). The IGM-δg^{inter} based isosurface colored blue and green signifies the interaction between bonded atomic basins that are strong and weak/vdW attractions, respectively, and that colored red is indicative of repulsion.

There is evidently C–Bi···Bi–C pnictogen bonding in ($O[(CH_2)_2BiPh_2]_2$) (Fig. S19a), but not in the other two systems. Although Bi in this system is positive, the Bi···Bi interaction is the result of attraction between two sites of different electron density. This is also evident from the angle of interaction, ∠C–Bi···Bi = 166.7°. Moreover, the Bi···Bi bond distance, 4.346 Å, is longer than the (C)Bi···O contact distances, yet it is much smaller than the sum of the vdW radii of the two Bi atomic basins (5.08 Å). Nevertheless, these are not the key driving forces responsible for the molecular packing in the crystals. There are C–H···O/C–H···S and C–H···π(C_6), –CH_2···C(π) and various π···π stacking interactions that drive the packing in the solid state (not shown).

S.G Bi- and Sb-centered Pnictogen Bonds in Functional materials

Another set of examples that involve linear or zigzag 1D chain-like architectures formed of pentagonal pyramidal MX_3^{2-} dianions in an environment of organic dications is shown in Fig S20a-e. The same topology of M···X and M–X bonding modes noted above is seen in these systems.

Probably one of the most important hybrid organic-inorganic materials for photovoltaics is $MAPbI_3$ (MA = methylammonium). While $MAPbI_3$ has been an important photovoltaic material, it is unstable and toxic, and hence environmentally unfriendly. Many attempts have been made to discover lead-free halide-based perovskites for photovoltaics and other optoelectronic applications. Several antimony- and bismuth-based halide perovskites have been synthesized and reported which may have future potential as perovskite-based solar-cell absorbers because of their lower toxicity. For instance, Wang and co-workers recently reported a lead-free, pseudo-3D perovskite optoelectronic material, $(MV)BiI_5$.[99] Although the authors have assigned the pentaiodobismuth cation to have a charge of +2, and noted that there are I···I contacts in the crystal, this may be misleading. Our analysis suggests that the methylviologen units act as spacers between the $[BiI_5]^{2-}$ quasi-linear chains along the crystallographic *a*-axes, and $[BiI_5]$ carries a charge of –2. The Bi···I links between the $[BiI_5]^{2-}$ units causing the 1D pseudo-linear chains are longer than the Bi–I bonds (*r*(Bi…I) values 3.665 Å *vs.* 2.873 Å). As explained above, the former links are typical of non-covalent interactions and the latter are bonds with mixed ionic and covalent character. Since the $[BiI_5]^{2-}$ units that cause the development of the long-range non-covalent interactions are entirely negative and there are no positive sites involved in making these interactions, it would be misleading to name the Bi···I links as pnictogen bonds even though they feature a directionality synonymous with Type-IIa pnictogen bonds. Because of this, we characterize them as Type-III pnictogen bonds. There are I···I links between linear chains in the crystal. They are very long (*r*(I…I) = 4.082 and 4.112 Å), slightly longer than twice the vdW radius of I, and more directional than the Bi···I long bonds. These, together with π···I interactions between MV^{2+} and $[BiI_5]^{2-}$, probably engineer the overall structure of the crystal system as pseudo three dimensional.

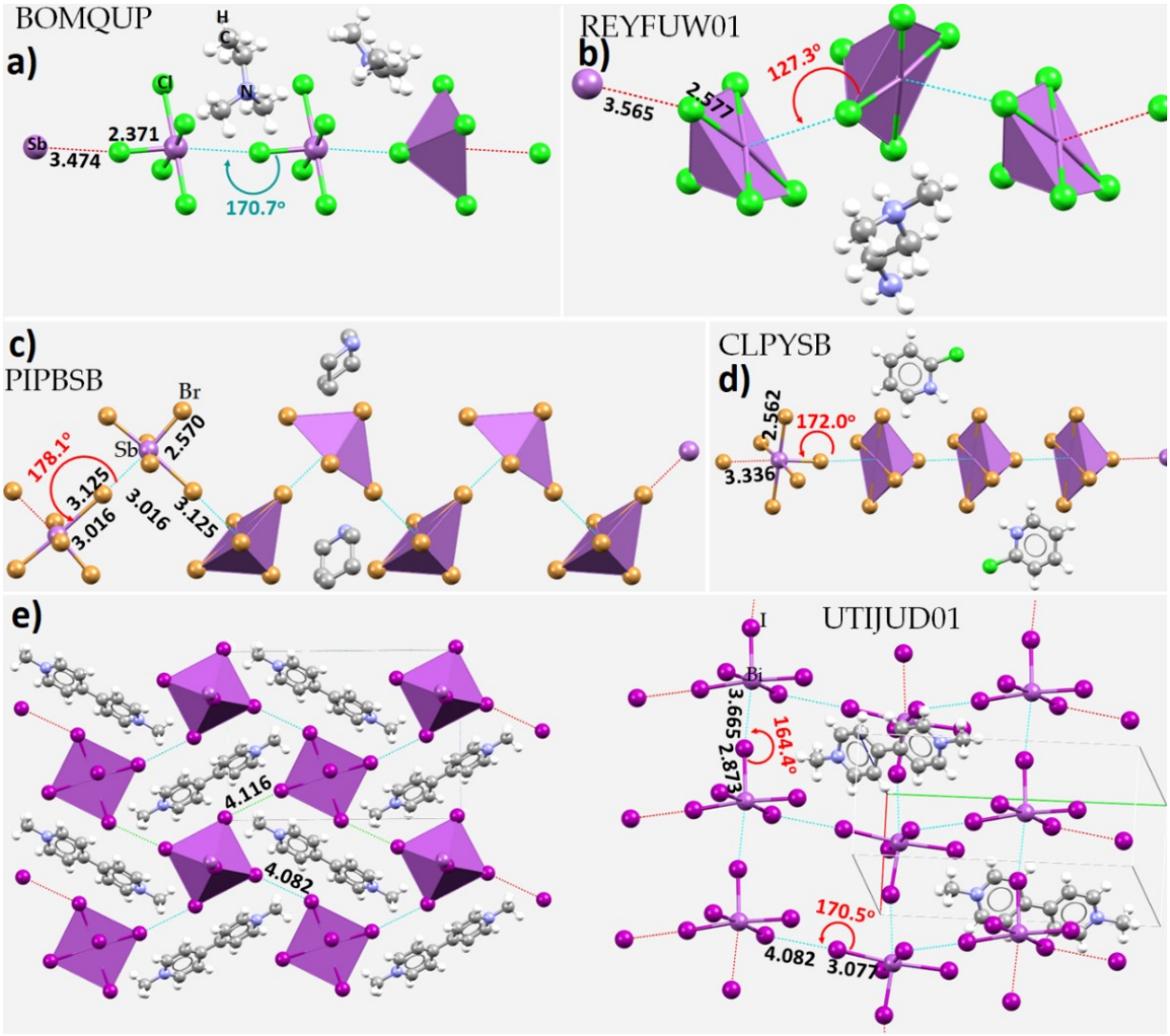

Figure S20. Further examples of hybrid organic anion-inorganic cation systems that feature 1D and 3D $[PnX_5]^{2n-}$ architectures though pnictogen-centered non-covalent links between the $[PnX_5]^{2-}$ entities. a) [En][$SbCl_5$] (En = $[C_2H_4(NH_3)_2]^{2+}$;[100] b) [$(CH_3)_2$En][$SbCl_5$] ($(CH_3)_2$En = $[(CH_3)_2NHCH_2CH_2NH_3]^{2+}$[101] c) $(Pip)_2[SbBr_5]$ (Pip = piperidinium);[102] [2Cl-py][$SbBr_5$];[103]; and e) (MV)[BiI_3].[99]

The (MV)BiI_5 perovskite has a narrow band gap of 1.48 eV, electrical conductivity of 0.73×10^{-10} S cm^{-1} and a better photoresponse than (MV)$BiCl_5$, with its 1 D structure formed by the non-covalent links between the $[BiCl_5]^{2-}$ units, and which has a bandgap of 2.59 eV. Comparable 1D systems include (TMP)[$BiCl_5$], (TMP)[$BiBr_5$] (TMP = tetramethylpiperazine)[104] and (DMEDA)BiI_5 (DMEDA^{2+} = $CH_3NH_3CH_2CH_2NH_3CH_3^{2+}$)[105]; they have bandgaps of 3.21, 2.67 and 1.82 eV, respectively. It was suggested in those studies that (MV)BiI_5 is the first Bi-based perovskite compound with a band gap energy comparable with $(CH_3NH_3)PbI_3$, which is encouraging for optoelectronic applications. This perovskite may open a pathway to

the design of pseudo-3D Bi-based perovskites with performance comparable with the widely examined $APbX_3$ absorbers.

S. H The Crystals of Bismuth

Crystals of Bi in several phases, both in 2D and 3D, with space groups *R-3m*, $P2_1/n$, $P2_1/m$, I_4/mcm, I_4/mmm, $Pm\text{-}\bar{3}m$, $Im\text{-}\bar{3}m$, *Cmca*, and C_2/m have been deposited in the ICSD. Stable, free-standing, 2D single-layer phases of Bi, called bismuthene, have been reported, including, for example, the buckled honeycomb or hexagonal (h-Bi), symmetric washboard (w-Bi), asymmetric washboard (aw-Bi), and square-octagon (so-Bi) structures; aw-Bi is less stable than w-Bi.[106]

The rhombohedral A7 structure of Bi is stabilized by Jones–Peielrs distortion.[107] It has two atoms in a primitive cell. The bulk bismuth with *R-3m* space group[107] has a layered structure. Each atom bonds covalently to its three nearest neighbors forming buckled bilayer with a σ bond, a characteristic of pnictogen bonding in a semimetal.[108] The interaction between the adjacent bilayers is much weaker than the intra-bilayer bonding; hence bismuth cleaves along the (111) plane.

Shown in Fig. S21a-c is the structure of Bi in the *R-3m* space group. The coordinately bound Bi in a given layer links with the equivalent atom in the neighboring layers by means of long-range contacts. Depending on the number of layers and packing of atoms in the unit-cell, the inter-layer distance between the monolayers can be determined. In the structure shown in Fig. S21a-b, the Bi···Bi inter-layer distance is 3.529 Å; each covalently bonded Bi site in a monolayer is linked with three nearest neighbors forming three Bi···Bi equivalent contacts that are directional (∠Bi–Bi···Bi) = 169.3°). These are non-covalent interactions. This view is justified since the coordinate bond formed by each Bi atom in each monolayer is 3.071 Å, which is markedly shorter than the long bonds just noted, and Bi is locally trigonal within a monolayer (if one ignores the presence of its stereo-active lone-pairs). Although the directional feature of the Bi···Bi links in the crystal is consistent with a Type-IIa interaction, the long-range interactions could be characterized as Type-III (Scheme 1) given the electrostatic potential on the Bi site is entirely positive. This conclusion is supported by the MESP of a Bi_2 molecule, computed with MP2/Aug-cc-pVTZ (Fig. S21d). The outer cap on Bi along the Bi–Bi bond extensions is positive with a local minimum of potential $V_{S,min}$ = 4.9 kcal mol^{-1}. The lateral portions of the same atom is described by a belt of positive potential ($V_{S,max}$ = 7.1 kcal mol^{-1}). The bonding region is described by a belt of negative potential ($V_{S,min}$ = –3.2 kcal mol^{-1}). These were 5.0, 7.1 and –3.4 kcal mol^{-1} with MP2/def2-TZVPPD, suggesting that the magnitude, but not the sign, of the potential is marginally affected by changing the size

of the pseudopotential. Clearly, the quasi-linearity of Bi···Bi close-contacts originates from the attraction between regions on Bi of unequal charge density, i.e., the portions with $V_{S,min}$ and $V_{S,max}$ along and around one Bi in a monolayer are attracting the opposite portions described by $V_{S,max}$ and $V_{S,min}$ on the same atom in the interacting monolayer, respectively. While this conclusion is drawn using the potentials computed on the fully relaxed geometry of the Bi_2 molecule that has an *r*(Bi–Bi) of 2.675 Å (and 2.663 Å) with MP2/Aug-cc-pVTZ (MP2/def2-TZVPPD), each monolayer in the crystal has an *r*(Bi–Bi) of is 3.071 Å. Our single point calculation with MP2/Aug-cc-pVTZ using the crystal geometry of Bi_2 has altered $V_{S,min}$ to $V_{S,max}$ on the surface of the Bi atom along the bond extensions with $V_{S,max}$ = 7.1 kcal mol^{-1}, but the character of $V_{S,min}$ ($V_{S,min}$ = –3.2 kcal mol^{-1}) remains unchanged at the bonding region. Further elongation of *r*(Bi–Bi) close to *r*(Bi···Bi) = 3.529 Å resulted in an MESP shown in Fig. S21e. While the surface region of the molecule is dissected into lateral and axial regions of positive potentials, the charge density at the bonding region is largely depleted, giving rise to a belt a positive potential. This is not unexpected since elongated molecules have mobile electron density, increasing their polarizability, and thus strengthening the dispersion forces between the bonded atomic basins.

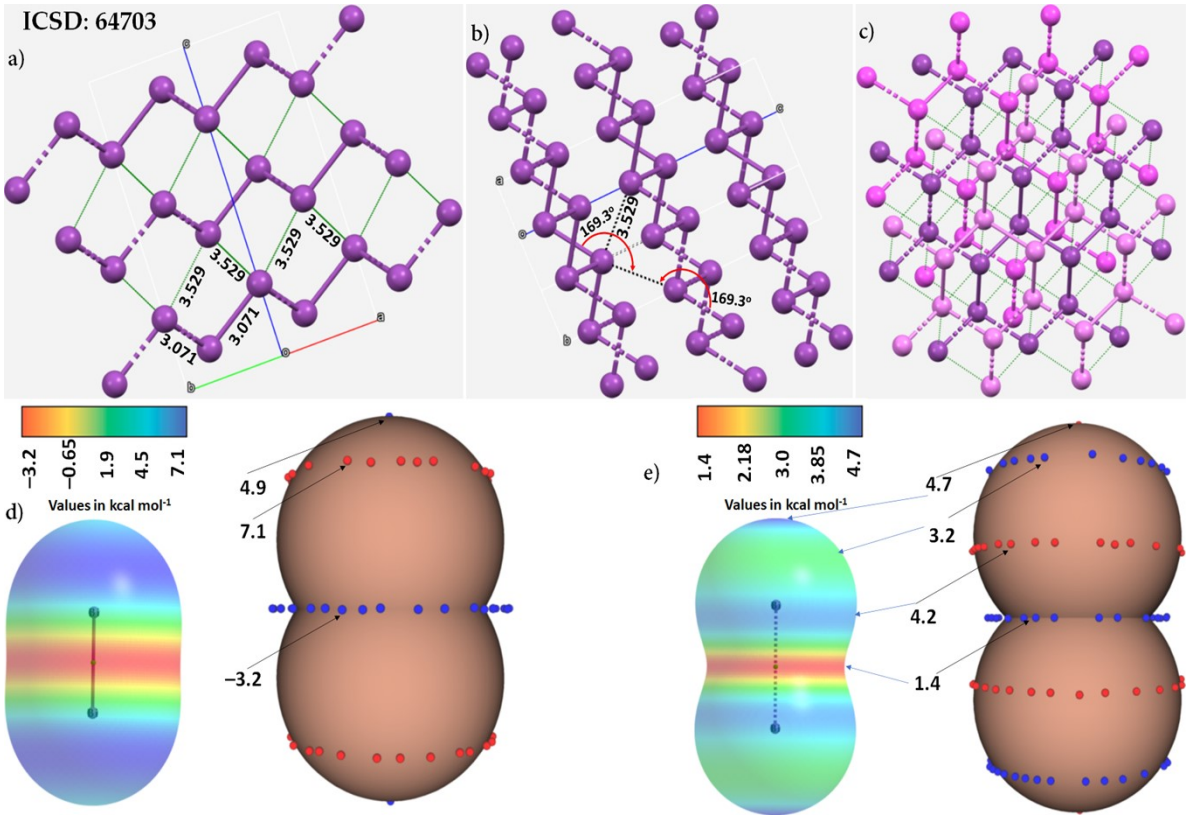

Figure S21. a)-c) Ball-and-stick model of three different views of the crystal of Bi (space group: *R-3m*), showing the inter-layer interactions between the bonded Bi sites that hold the monolayers together. b) Illustration of the typical nature of link formed by a given Bi site in a monolayer with three nearest neighbor Bi sites in a neighboring monolayer. c) Illustration of Bi···Bi contacts formed by each Bi site in each of the three layers (the three layers colored in purple, pink and faint-pink, respectively). The thin dotted lines between Bi sites represent Bi···Bi close contacts. Selected bond distances and bond angles are in Å and degree, respectively. d) and e) The MP2/Aug-cc-pVTZ level 0.001 a.u. isoelectron density envelope mapped potential on the surface of a Bi_2 molecule calculated on the MP2/Aug-cc-pVTZ optimized and (fixed) crystal geometries, respectively. The tiny blue and red dots on van der Waals surfaces of Bi_2 (right) represent the local most minimum and local most maximum of potential, respectively. The ICSD ref. for the crystal is shown in a).

References (to material in the ESI)

1. G. R. Desiraju and T. Steiner, *The weak hydrogen bond in structural chemistry and biology (International Union of Crystallography Monographs on Crystallography, 9)*, Oxford University Press, Oxford and New York, 1999.
2. A. Gavezzotti, *J. Am. Chem. Soc.*, 1983, **105**, 5220-5225.
3. D. M. P. Mingos and A. L. Rohl, *J. Chem. Soc., Dalton Trans.*, 1991, DOI: 10.1039/DT9910003419, 3419-3425.
4. S. Alvarez, *Dalton Trans.*, 2013, **42**, 8617-8636.
5. M. Kazmierczak and A. Katrusiak, *Acta Crystallogr. B*, 2019, **75**, 865-869.
6. J. Dunitz, *IUCrJ*, 2015, **2**, 157-158.
7. P. R. Varadwaj, A. Varadwaj, H. M. Marques and K. Yamashita, *Compounds*, 2022, **2**, 80-110.
8. P. R. Varadwaj, A. Varadwaj, H. M. Marques and K. Yamashita, *Molecules*, 2022, **27**, 1487.
9. A. Varadwaj, P. R. Varadwaj, H. M. Marques and K. Yamashita, *Molecules*, 2022, **27**, 3421.
10. A. Varadwaj, P. R. Varadwaj, H. M. Marques and K. Yamashita, *Int. J. Mol. Sci.*, 2022, **23**, 4674.
11. G. P. Schiemenz, *Z. Naturforsch. B*, 2007, **62**, 235-243.
12. P. Politzer and J. S. Murray, *Struct. Chem.*, 2021, **32**, 623-629.
13. I. Dance, *New J. Chem.*, 2003, **27**, 22-27.
14. I. Y. Chernyshov, I. V. Ananyev and E. A. Pidko, *ChemPhysChem*, 2020, **21**, 370-376.
15. P. R. Varadwaj, A. Varadwaj and H. M. Marques, *Inorganics*, 2019, **7**, 40.
16. M. A. A. Ibrahim and N. A. M. Moussa, *ACS Omega*, 2020, **5**, 21824-21835.
17. M. J. Frisch, M. Head-Gordon and J. A. Pople, *Chem. Phys. Lett.*, 1990, **166**, 275-280.
18. M. Head-Gordon and T. Head-Gordon, *Chem. Phys. Lett.*, 1994, **220**, 122-128.
19. B. P. Pritchard, D. Altarawy, B. Didier, T. D. Gibson and T. L. Windus, *J. Chem. Inf. Model.*, 2019, **59**, 4814-4820.
20. M. J. Frisch, G. W. Trucks, H. B. Schlegel, G. E. Scuseria, M. A. Robb, J. R. Cheeseman, G. Scalmani, V. Barone, G. A. Petersson, H. Nakatsuji, X. Li, M. Caricato, A. V. Marenich, J. Bloino, B. G. Janesko, R. Gomperts, B. Mennucci, H. P. Hratchian, J. V. Ortiz, A. F. Izmaylov, J. L. Sonnenberg, Williams, F. Ding, F. Lipparini, F. Egidi, J. Goings, B. Peng, A. Petrone, T. Henderson, D. Ranasinghe, V. G. Zakrzewski, J. Gao, N. Rega, G. Zheng, W. Liang, M. Hada, M. Ehara, K. Toyota, R. Fukuda, J. Hasegawa, M. Ishida, T. Nakajima, Y. Honda, O. Kitao, H. Nakai, T. Vreven, K. Throssell, J. A. Montgomery Jr., J. E. Peralta, F. Ogliaro, M. J. Bearpark, J. J. Heyd, E. N. Brothers, K. N. Kudin, V. N. Staroverov, T. A. Keith, R. Kobayashi, J. Normand, K. Raghavachari, A. P. Rendell, J. C. Burant, S. S. Iyengar, J. Tomasi, M. Cossi, J. M. Millam, M. Klene, C. Adamo, R. Cammi, J. W. Ochterski, R. L. Martin, K. Morokuma, O. Farkas, J. B. Foresman and D. J. Fox, *Journal*, 2016.
21. P. Politzer, J. S. Murray, T. Clark and G. Resnati, *Phys. Chem. Chem. Phys.*, 2017, **19**, 32166-32178.
22. P. Politzer, J. S. Murray and T. Clark, *Phys. Chem. Chem. Phys.*, 2021, **23**, 16458-16468.
23. P. Politzer, J. S. Murray and T. Clark, *Phys. Chem. Chem. Phys.*, 2010, **12**, 7748-7757.
24. T. Clark, M. Hennemann, J. S. Murray and P. Politzer, *J. Mol. Model.*, 2007, **13**, 291-296.
25. J. S. Murray, P. Lane, T. Clark, K. E. Riley and P. Politzer, *J. Mol. Model.*, 2012, **18**, 541-548.
26. P. Politzer and J. S. Murray, *Crystals*, 2017, **7**, 212, doi:210.3390/cryst7070212.
27. P. R. Varadwaj, A. Varadwaj and B.-Y. Jin, *Phys. Chem. Chem. Phys.*, 2015, **17**, 31624-31645.
28. P. R. Varadwaj, A. Varadwaj, H. M. Marques and K. Yamashita, *Computation*, 2018, **6**, 51.
29. C. Lefebvre, G. Rubez, H. Khartabil, J.-C. Boisson, J. Contreras-García and E. Hénon, *Phys. Chem. Chem. Phys.*, 2017, **19**, 17928-17936.
30. C. Lefebvre, H. Khartabil, J.-C. Boisson, J. Contreras-García, J.-P. Piquemal and E. Hénon, *ChemPhysChem*, 2018, **19**, 724-735.
31. R. F. Bader, *Atoms in Molecules: A Quantum Theory*, Oxford University Press, Oxford, 1990.
32. C. F. Macrae, I. J. Bruno, J. A. Chisholm, P. R. Edgington, P. McCabe, E. Pidcock, L. Rodriguez-

Monge, R. Taylor, J. van de Streek and P. A. Wood, *J. Appl. Cryst.*, 2008, **41**, 466-470.
33. W. Humphrey, A. Dalke and K. Schulten, *J. Molec. Graphics*, 1996, **14**, 33-38.
34. T. A. Keith, *Journal*, 2019.
35. T. Lu and F. Chen, *J. Comp. Chem.*, 2012, **33**, 580-592.
36. Z. Ouerghi, M. A. Fersi, S. Elleuch, T. Roisnel, A. Othmani and R. Kefi, *J. Clust. Sci.*, 2021, **32**, 179-191.
37. Z. Deng, F. Wei, Y. Wu, R. Seshadri, A. K. Cheetham and P. Canepa, *Inorg. Chem.*, 2020, **59**, 3377-3386.
38. J. Sanderson and C. A. Bayse, *Tetrahedron*, 2008, **64**, 7685-7689.
39. A. M. Toma, A. Pop, A. Silvestru, T. Rüffer, H. Lang and M. Mehring, *Dalton Trans.*, 2017, **46**, 3953-3962.
40. F. Yuepeng, X. Hongwei, Z. Zhongyuan and Y. Kaibei, *Jiegou Huaxue*, 1988, **7**, 196
41. B. Liu, L. Xu, G.-C. Guo and J.-S. Huang, *J. Sol. State Chem.*, 2006, **179**, 1611-1617.
42. F. Lambarki, A. Ouasri, H. Zouihri and A. Rhandour, *J. Mol. Struct.*, 2017, **1142**, 275-284.
43. K. H. Whitmire, in *Encyclopedia of Inorganic and Bioinorganic Chemistry*, DOI: https://doi.org/10.1002/9781119951438.eibc0018.pub2, pp. 1-32.
44. W. Frank and V. Reiland, *Acta Cryst. C*, 1998, **54**, 1626-1628.
45. B. Wagner, F. Weigend and J. Heine, *Inorg. Chem.*, 2021, **60**, 4352-4356.
46. P. Manna, D. Szücs, T. Csupász, A. Fekete, D. Szikra, Z. Lin, A. Gáspár, S. Bhattacharya, A. Zulaica, I. Tóth and U. Kortz, *Inorg. Chem.*, 2020, **59**, 16769-16782.
47. X. Hu, J. Wang, W. Mao, G. Zheng, S. Mo, N. Tian, B. Zhou, F. Long and Z. Zou, *ChemistrySelect*, 2021, **6**, 1099-1106.
48. A. S. Antsyshkina, M. A. Porai-Koshits and V. N. Ostrikova, *Russ. J. Coord. Chem.*, 1983, **9**, 1118-1120.
49. A. Finelli, S.-L. Abram, N. Hérault, A. Crochet and K. M. Fromm, *Cryst. Growth & Design*, 2020, **20**, 4945-4958.
50. J. Ramler and C. Lichtenberg, *Dalton Trans.*, 2021, **50**, 7120-7138.
51. K. H. Whitmire, M. R. Churchill and J. C. Fettinger, *J. Am. Chem. Soc.*, 1985, **107**, 1056-1057.
52. S. Martinengo and G. Ciani, *J. Chem. Soc., Chem. Commun.*, 1987, DOI: 10.1039/C39870001589, 1589-1591.
53. V. V. Sharutin, I. V. Egorova, N. N. Klepikov, E. A. Boyarkina and O. K. Sharutina, *Russ. J. Inorg. Chem.*, 2009, **54**, 1768.
54. M. Shieh, Y.-H. Liu, C.-Y. Huang, S.-W. Chen, W.-K. Cheng and L.-T. Chien, *Inorg. Chem.*, 2019, **58**, 6706-6721.
55. F. Calderazzo, A. Morvillo, G. Pelizzi, R. Poli and F. Ungari, *Inorg. Chem.*, 1988, **27**, 3730-3733.
56. M. Jurrat, L. Maggi, W. Lewis and L. T. Ball, *Nature Chem.*, 2020, **12**, 260-269.
57. M. Hejda, R. Jirásko, A. Růžička, R. Jambor and L. Dostál, *Organometallics*, 2020, **39**, 4320-4328.
58. T. Murafuji, M. Nagasue, Y. Tashiro, Y. Sugihara and N. Azuma, *Organometallics*, 2000, **19**, 1003-1007.
59. J. Ramler, J. Poater, F. Hirsch, B. Ritschel, I. Fischer, F. M. Bickelhaupt and C. Lichtenberg, *Chem. Sci.*, 2019, **10**, 4169-4176.
60. S. Arlt, J. Harloff, A. Schulz, A. Stoffers and A. Villinger, *Inorg. Chem.*, 2016, **55**, 12321-12328.
61. V. V. Sharutin, O. K. Sharutina and V. S. Senchurin, *J. Struct. Chem.*, 2020, **61**, 734-741.
62. S. S. Batsanov, *Inorg. Mater.*, 2001, **37**, 871-885.
63. V. V. Sharutin, O. K. Sharutina and A. N. Efremov, *Russ. J. Coord. Chem.*, 2021, **47**, 626-630.
64. S. L. Benjamin, L. Karagiannidis, W. Levason, G. Reid and M. C. Rogers, *Organometallics*, 2011, **30**, 895-904.
65. M. Olaru, S. Krupke, E. Lork, S. Mebs and J. Beckmann, *Dalton Trans.*, 2019, **48**, 5585-5594.
66. E. Silina, Y. Bankovsky, V. Belsky, A. Stash and J. Ashaks, *Latv. Khim. Z.*, 1998, 101-104
67. A. Gehlhaar, C. Wölper, F. van der Vight, G. Jansen and S. Schulz, *Eur. J. Inorg. Chem.*, 2022, **2022**,

e202100883.
68. M. Kimura, A. Iwata, M. Itoh, K. Yamada, T. Kimura, N. Sugiura, M. Ishida and S. Kato, *Helv. Chim. Acta*, 2006, **89**, 747-783.
69. S. Schulz, A. Kuczkowski, D. Bläser, C. Wölper, G. Jansen and R. Haack, *Organometallics*, 2013, **32**, 5445-5450.
70. Z. Li, D. Ouyang and L. Xu, *Chem. Commun.*, 2019, **55**, 6783-6786.
71. A. J. Plajer, A. L. Colebatch, F. J. Rizzuto, P. Pröhm, A. D. Bond, R. García-Rodríguez and D. S. Wright, *Angew Chem. Int. Edn.*, 2018, **57**, 6648-6652.
72. N. L. Kilah, S. Petrie, R. Stranger, J. W. Wielandt, A. C. Willis and S. B. Wild, *Organometallics*, 2007, **26**, 6106-6113.
73. Á. García-Romero, A. J. Plajer, D. Miguel, D. S. Wright, A. D. Bond, C. M. Álvarez and R. García-Rodríguez, *Inorg. Chem.*, 2020, **59**, 7103-7116.
74. T. Svoboda, R. Jambor, A. Růžička, Z. Padělková, M. Erben, R. Jirásko and L. Dostál, *Eur. J. Inorg. Chem.*, 2010, **2010**, 1663-1669.
75. S. Furan, E. Hupf, E. Lork and J. Beckmann, *Rev. Roum. Chim.*, 2020, **65**, 673.
76. P. S. Nejman, T. E. Curzon, M. Bühl, D. McKay, J. D. Woollins, S. E. Ashbrook, D. B. Cordes, A. M. Z. Slawin and P. Kilian, *Inorg. Chem.*, 2020, **59**, 5616-5625.
77. B. A. Chalmers, C. B. E. Meigh, P. S. Nejman, M. Bühl, T. Lébl, J. D. Woollins, A. M. Z. Slawin and P. Kilian, *Inorg. Chem.*, 2016, **55**, 7117-7125.
78. P. Pérez-Lourido, L. Valencia, J. Romero, J. A. García-Vázquez, A. Sousa and J. Zubieta, *Polyhedron*, 2012, **45**, 200-203.
79. N. W. Alcock, M. Ravindran and G. R. Willey, *J. Chem. Soc., Chem. Commun.*, 1989, DOI: 10.1039/C39890001063, 1063-1065.
80. G. R. Willey, D. R. Aris and W. Errington, *Inorg. Chim. Acta*, 2000, **300-302**, 1004-1013.
81. N. W. Alcock, M. Ravindran and G. R. Willey, *Acta Crystallogr. B*, 1993, **49**, 507-514.
82. B. Wagner and J. Heine, *Z. Anorg. Allg. Chem.*, 2021, **647**, 663-666.
83. A. Varadwaj, P. R. Varadwaj, H. M. Marques, K. Yamashita and H. M. M. Pradeep R. Varadwaj, Koichi Yamashita, , , *arXiv:1802.09995 [physics.chem-ph] (https://arxiv.org/abs/1802.09995).* 2017.
84. C. Fiolka, M. Richter, I. Pantenburg, A.-V. Mudring and G. Meyer, *Crystals*, 2011, **1**, 220-228.
85. H. J. Breunig and H. Althaus, *Phosphorus, Sulfur, and Silicon and the Related Elements*, 2001, **168**, 123-128.
86. W.-Y. Yin, Y.-G. Weng, M. Jiang, S.-K. Yu, Q.-Y. Zhu and J. Dai, *Inorg. Chem.*, 2020, **59**, 5161-5169.
87. W. Clegg, R. J. Errington, G. A. Fisher, R. J. Flynn and N. C. Norman, *J. Chem. Soc., Dalton Trans.*, 1993, DOI: 10.1039/DT9930000637, 637-641.
88. Y. Matano, N. Azuma and H. Suzuki, *J. Chem. Soc., Perkin 1*, 1994, DOI: 10.1039/P19940001739, 1739-1747.
89. H. Sommer, A. Eichhöfer and D. Fenske, *Zeit. Anorg. Allg. Chem.*, 2008, **634**, 436-440.
90. J. E. Waters, G. Berger, A. J. Peel, R. García-Rodríguez, A. D. Bond and D. S. Wright, *Chem. Eur. J.*, 2021, **27**, 12036-12040.
91. S. Solyntjes, B. Neumann, H.-G. Stammler, N. Ignat'ev and B. Hoge, *Eur. J. Inorg. Chem.*, 2016, **2016**, 3999-4010.
92. S. Wallenhauer, D. Leopold and K. Seppelt, *Inorg. Chem.*, 1993, **32**, 3948-3951.
93. J. E. Walley, L. S. Warring, G. Wang, D. A. Dickie, S. Pan, G. Frenking and R. J. Gilliard Jr., *Angew Chem. Int. Edn.*, 2021, **60**, 6682-6690.
94. X.-W. Zhang, J. Xia, H.-W. Yan, S.-L. Luo, S.-F. Yin, C.-T. Au and W.-Y. Wong, *J. Organomet. Chem.*, 2009, **694**, 3019-3026.
95. A. M. Preda, W. B. Schneider, M. Rainer, T. Rüffer, D. Schaarschmidt, H. Lang and M. Mehring, *Dalton Trans.*, 2017, **46**, 8269-8278.
96. M. Hunger, C. Limberg and P. Kircher, *Angew Chem. Int. Edn.*, 1999, **38**, 1105-1108.
97. H. Althaus, H. J. Breunig and E. Lork, *Organometallics*, 2001, **20**, 586-589.

98. M. N. Bochkarev, G. A. Razuvaev, L. N. Zakharov and Y. T. Struchkov, *J. Organomet. Chem.*, 1980, **199**, 205-216.
99. Y. Wang, R. Wen, Y. Liu, L.-Y. Bi, M. Yang, H. Sun, Y.-Z. Zheng, G. Zhang and Z. Gao, *ChemSusChem*, 2020, **13**, 2753-2760.
100. M. Bujak and J. Zaleski, *Acta Crystallogr. C*, 1999, **55**, 1775-1778.
101. M. Bujak and R. J. Angel, *J. Phys. Chem. B*, 2006, **110**, 10322-10331.
102. H. A. Abdel-Rehim and E. A. Meyers, *Cryst. Struct. Commun.*, 1973, **2**, 45-49.
103. J. M. Carola, D. D. Freedman, K. L. McLaughlin, P. C. Reim, W. J. Schmidt, R. G. Haas, W. J. Broome, E. A. DeCarlo and S. L. Lawton, *Cryst. Struct. Commu*, 1976, **5**, 393-395.
104. J. K. Pious, A. Katre, C. Muthu, S. Chakraborty, S. Krishna and C. Vijayakumar, *Chem. Mater.*, 2019, **31**, 1941-1945.
105. L. Yao, G. Niu, L. Yin, X. Du, Y. Lin, X. Den, J. Zhang and J. Tang, *J. Mater. Chem. C*, 2020, **8**, 1239-1243.
106. Y. Kadioglu, S. B. Kilic, S. Demirci, O. Ü. Aktürk, E. Aktürk and S. Ciraci, *Phys. Rev. B*, 2017, **96**, 245424.
107. Q. Li, H. Zhu, L. Zheng, L. Fan, Y. Ren, J. Chen, J. Deng and X. Xing, *Adv. Sci.*, 2016, **3**, 1600108.
108. M.-Y. Liu, Y. Huang, Q.-Y. Chen, Z.-Y. Li, C. Cao and Y. He, *RSC Adv.*, 2017, **7**, 39546-39555.